INL/RPT-23-74615-Revision-0

Validation and Verification of TEDS Facility HYBRID Modeling

September 2023

Vaclav Novotny, Junyung Kim, Terry James Morton, Sarah Elizabeth Creasman, Daniel Mark Mikkelson

Changing the World's Energy Future

Idaho National Laboratory

INL is a U.S. Department of Energy National Laboratory operated by Battelle Energy Alliance, LLC

INL/RPT-23-74615-Revision-0

Validation and Verification of TEDS Facility HYBRID Modeling

Vaclav Novotny, Junyung Kim, Terry James Morton, Sarah Elizabeth Creasman, Daniel Mark Mikkelson

September 2023

Idaho National Laboratory
Idaho Falls, Idaho 83415

http://www.inl.gov

Prepared for the
U.S. Department of Energy
Under DOE Idaho Operations Office
Contract DE-AC07-05ID14517

INL/RPT-23-74615
Revision 0

Validation and Verification of TEDS Facility HYBRID Modelling

September | 2023

Vaclav Novotny, Junyung Kim, Terry J. Morton, Sarah Creasman, Daniel Mikkelson

Idaho National Laboratory

IES
Integrated Energy Systems

INL is a U.S. Department of Energy National Laboratory operated by Battelle Energy Alliance, LLC

INL/RPT-23-74615
Revision 0

Validation and Verification of TEDS Facility HYBRID Modelling

**Vaclav Novotny, Junyung Kim, Terry J. Morton,
Sarah Creasman, Daniel Mikkelson**

September | 2023

**Idaho National Laboratory
Integrated Energy Systems
Idaho Falls, Idaho 83415**

http://www.ies.inl.gov

**Prepared for the
U.S. Department of Energy
Office of Nuclear Energy
Under DOE Idaho Operations Office
Contract DE-AC07-05ID14517**

Page intentionally left blank.

ABSTRACT

The HYBRID repository is an Idaho National Laboratory (INL)-developed library of models for simulating select integrated energy systems. Starting in 2015, HYBRID models have been developed to describe the physical operation of tightly coupled thermal systems such as power generators, thermal transport systems, thermal energy storage (TES), and thermal-to-electric conversion systems. The present work demonstrates validation and verification (V&V) capabilities afforded by the Thermal Energy Distribution System (TEDS) at INL. Building on prior work, the TEDS model was updated and verified to better represent the actual system configuration and operating control system. An experimental test that primarily focused on thermocline tank performance was replicated. Several anomalies were found in the operation data pertaining to the experiment facility. V&V activities for calibrating selected input parameters were demonstrated on individual components. The calibration demonstration was then expanded to multiple components, as well as to a multi-parameter metric encompassing the entire system. The V&V methodology was successfully applied to validate the model with experimental data. It also confirmed a hypothesis regarding an anomaly seen in the experimental performance data.

Page intentionally left blank

CONTENTS

FIGURES

TABLES

ACRONYMS

DETAIL	Dynamic Energy Transport and Innovation Laboratory
DTW	Dynamic time warping
HX	Heat exchanger
INL	Idaho National Laboratory
MAGNET	Microreactor Agile Non-nuclear Test Bed
PCU	Power Conversion Unit
P&ID	Piping and instrumentation diagram
TEDS	Thermal Energy Distribution System
TES	Thermal energy storage
V&V	Verification and validation

Page intentionally left blank

1. INTRODUCTION

Verification and validation (V&V) work consists of two distinct steps. The first is to verify that the model results match the coded equation set, that the results match the outcomes anticipated based on expert insight, and that the model matches physical behavior, when applicable. The TEDS model has been verified in previous efforts [1]. Validation has been delayed due to operational delays in the experimental system. Minimal updates to the prior verification are presented in Section 2 of this report. The second step of V&V is to validate the model results using extra-model data—preferably, real-world data. Specific activities include adjusting and modifying the model, performing experimental activities and experimental data analyses, running validation codes such as dynamic time warping (DTW), and tuning the model parameters to match the physical data. The present report demonstrates the updated V&V of the Thermal Energy Distribution System (TEDS) HYBRID model at Idaho National Laboratory (INL) [1],[6]. V&V of the facility models in the HYBRID repository is needed to foster potential future activities involving digital twin analyses, real-time optimization, and remote operation and control [2-3].

This work relates to INL facilities that integrate real-time digital signals and mock nuclear power, thermal energy storage (TES), and industrial heat use via high-temperature electrolysis. The Dynamic Energy Transport and Integration Laboratory (DETAIL), seen in Figure 1, houses the Microreactor Agile Non-nuclear Experimental Test Bed (MAGNET) as well as TEDS. The work described in this report focuses on TEDS, which contains a thermocline TES system featuring thermal oil and solid alumina beads as the filling material, an electric heater, and a heat exchanger (HX) to reject heat (via an auxiliary circuit) into the ambient [4-5].

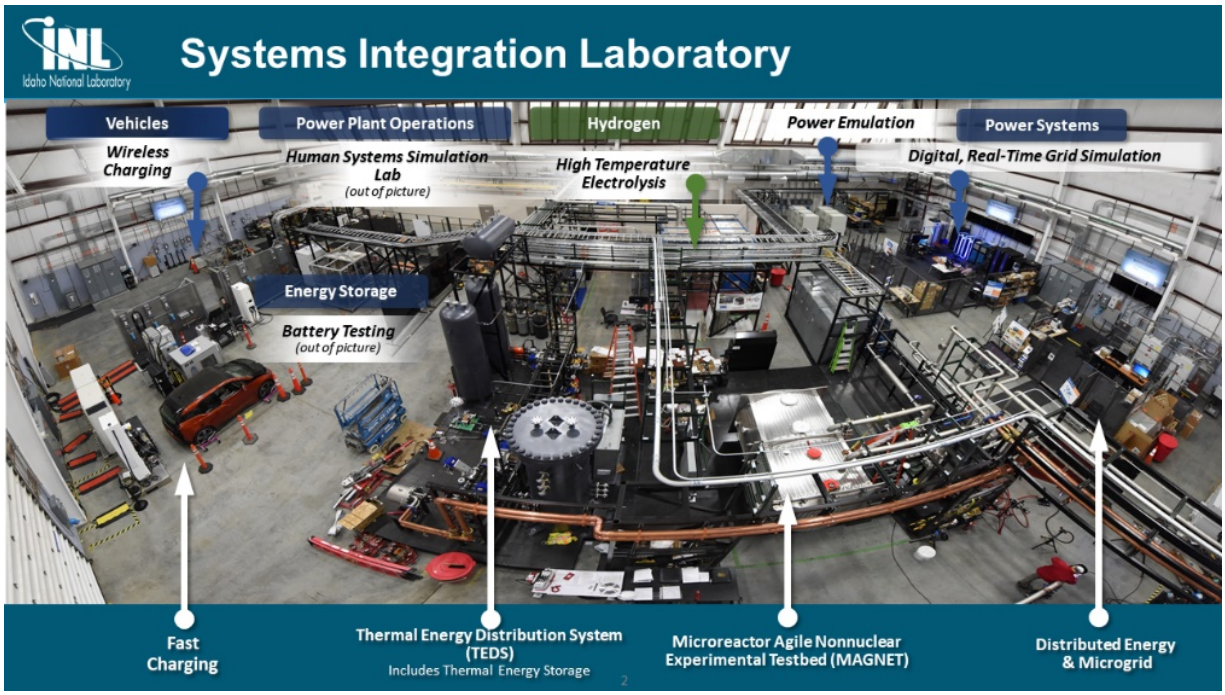

Figure 1. Wide-angle view of the Systems Integration Laboratory, which contains the DETAIL facility.

Modelica models, contributed to the HBYRID modeling repository, describe the dynamic behavior of DETAIL. Updated verification of the TEDS model within the HYBRID repository is included in this report. A majority of this report focuses on the validation of this model using experimental data produced in July of 2023. The validated TEDS model will be used across various integrated energy systems applications including control design, real-time optimization, and digital twin evaluation [1], [3], [6].

This report addresses the following activities:

- Verifying the DETAIL model to correct mismatches between the Modelica models and the updated physical configurations and control regime.
- Using new experimental data to validate the Modelica model using dynamic time warping (DTW).
- Development, updating, and implementation of new tools including DTW [1].
- Validation and/or tuning an individual models to match the reference values (e.g., tuning a HX to match the vendor specifications).
- Validation of a complex simulation model by comparing multiple parameters against the experimental results.
- Confirming a hypothesis explaining an anomaly observed in the experimental performance data.
- Performing an input parameter calibration to sufficiently match the simulation results to the experiment results based on differences explained by an observed anomaly.

The present work begins by comparing the preexisting models to the experimental system, then adjusts those models—by correcting the system configuration—to better match the experimental system. The control system in the TEDS model is also adjusted to enable replication of experimental runs (changing automated setpoint-based control to manual control). Utilizing the design parameters of a specific component, demonstrated on a heat exchanger size, the present work also provides a guideline how the models can be adjusted and validated to match nominal experimental performance.

Next, an experimental run of TEDS is outlined and the results analyzed. The model-experiment validation methodology is demonstrated by validating a hypothesis regarding a specific anomaly seen in the experimental performance data. General trends validating the hypothesis are illustrated on a single parameter within the thermocline. Then, the calibration demonstration was expanded to multiple components, encompassing the entire system.

Continued validation of the HYBRID TEDS model is necessary moving forward. Subsequent experimental data sets will be used to continue to validate the model.

2. SYSTEM VERIFICATION AND MODELS ADJUSTMENT

Verification of separate component models has been reported in previous work [1]. During verification of the models of experimental systems for this work, it was found that the physical layout (process diagram) did not correspond to the Modelica models of these systems.

Therefore, the HYBRID TEDS model was updated to better represent the installed system configuration and operating control system. Certain prior modeling assumptions were relaxed, and various errors corrected. The only clear phenomena not presently accounted for is the thermal loss of the piping to the environment (it is implemented in storage tank). Pipe heat loss could, if found essential, be added in the future to improve the accuracy of the TEDS model. As the operational method of TEDS will gradually evolve from human-governed to autonomously controlled, further changes to the control systems of the model are expected.

2.1 TEDS

One of the first updates to the TEDS model was changing the primary heat transfer fluid to the correct Therminol®-66 medium. A bypass line around the glycol HX was also added. Previously, the glycol-water mixture flowrate was controlled in the model to obtain a reference oil outlet temperature. In the experimental bay, the glycol-water mixture is pumped at a constant flowrate and temperature. Temperature control is accomplished by manually mixing the HX outlet and bypass line flows. The added bypass line and its corresponding control valve now enables the model to operate in like fashion. Due to the model complexity involved, successful implementation of this measure required adding a nonlinear break component to aid in the calculation by decreasing the stiffness of the system matrix. The piping and instrumentation diagram (P&ID) for TEDS (see Appendix A) shows the current physical layout, which is

now matched by the model. To adequately compare the model data with the experimental data, valve opening and temperature/flowrate setpoint controls were added in form of timetables. The flowrate within the model is controlled by setting valves to meet the volumetric flowrate setpoint. This approach serves as a proxy for the combined control (in the experiment) that specifies the variable-frequency drive pump frequency and—eventually—valve throttling. Overall, these changes do not change the operation verification that was done in the past [1]. Therefore, subsequent verification results are not included in this report to avoid redundancy.

For a feasible, more direct comparison between the experimental and the modelling data, the model configuration around the thermocline tank was altered to enable the temperature reading to be performed by a single sensor, both in charging and discharging mode. The modifications are shown highlighted by the purple boxes in Figure 2.

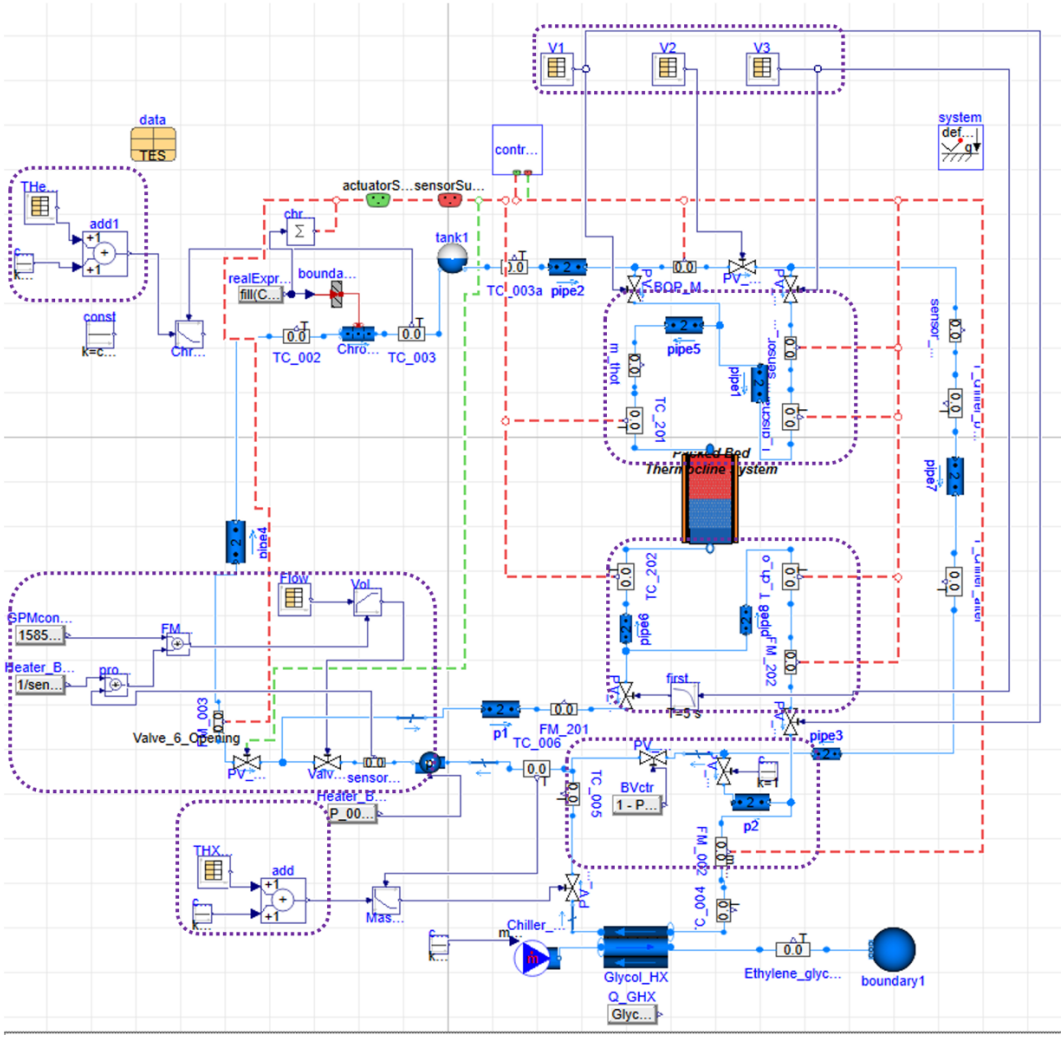

Figure 2. TEDS model, with the modified section highlighted in dotted purple boxes.

2.2 MAGNET

Major shortcomings were identified in the MAGNET Modelica model, as the model had not been updated regarding certain design changes. Installation of a recuperated Capstone C30 microturbine that has been converted for indirect heating [7] (otherwise known as a power conversion unit [PCU]) is planned for fiscal year 2024. The installation plan of the PCU interconnection to the rest of the MAGNET

system had been updated in the time since the modeling efforts were previously reported [6]. Figure 3 shows a section of the current model—highlighting the points of issue—as well as a detailed process diagram of the correct configuration. Correcting the previous errors in the model and verifying that the MAGNET-TEDS HX is properly sized and modeled are subjects for future effort.

As experimental data becomes available, a full verification and validation report should be generated for MAGNET operation. That evaluation should lead into combined MAGNET-TEDS operation, connected through the interfacing HX.

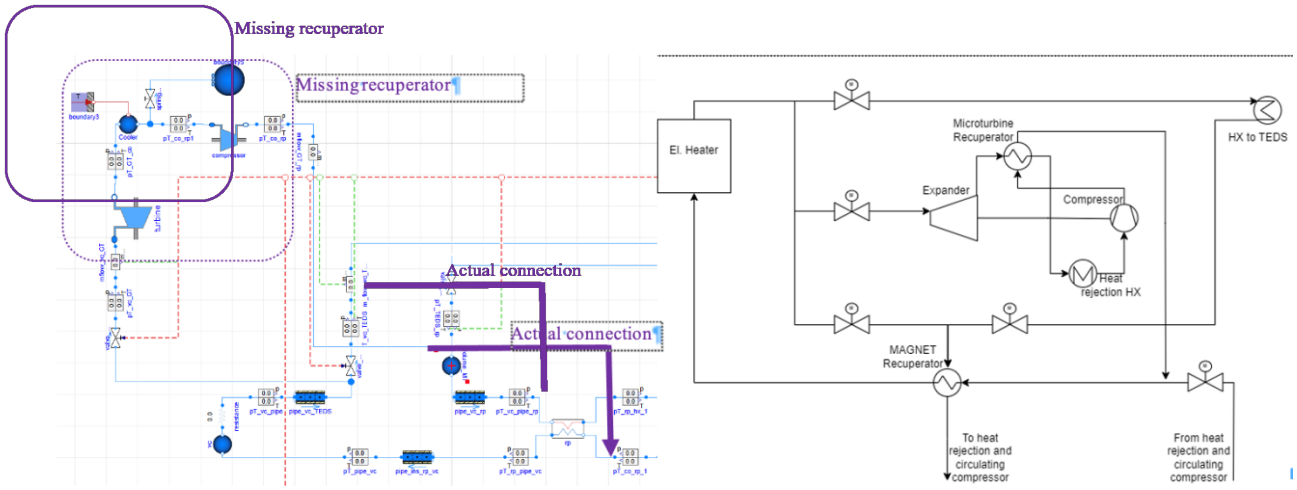

Figure 3. Current Modelica model and the correct configuration of the microturbine system in MAGNET.

2.3 Simulation Model Validation Using Dynamic Time Warping

Simulation model validation generally involves testing the computer program to ensure it meets specific requirements. Various metrics can be used to evaluate the code accuracy within a defined domain, in comparison to the level of accuracy required for the validation purpose. This validation process can be iterative, with new unique simulation data being acquired between iterations. If the performance is deemed insufficient, simulation model calibration is conducted to align it more closely with the experimental dataset. The updated model then undergoes the validation process once again.

To measure the level of agreement between the simulation data and the experiment data from the TEDS experiment, DTW distance was used as a validation metric. DTW presents a global minimization problem between the two time series of datasets, with each element of the first time series being contiguously linked to the closest matching element of the subsequent time series [1]. Unlike the Euclidean distance metric (simplistically, Equation [2], where x and y are measured at the same time index), DTW does not demand that the time series be of the same length. This makes it flexible in handling variations caused by system delays, computational expense, or measurement shifts [2]. Moreover, DTW can effectively manage types of outliers or noise that the standard Euclidean distance metric struggles to handle [3].

To align query (i.e., simulation, x) and reference sequences (i.e., experiment, y), the DTW algorithm first computes an n × m distance matrix given two multidimensional time series: $X = \{\mathbf{x}_1, \mathbf{x}_2, \ldots \mathbf{x}_i, \ldots \mathbf{x}_n\}$ and $Y = \{\mathbf{y}_1, \mathbf{y}_2, \ldots, \mathbf{y}_j, \ldots \mathbf{y}_m\}$ of length n and m, where the dimension of a vector $\mathbf{x}_i$ or $\mathbf{y}_j$ is P (i.e., $\mathbf{x}_i$ = (), as shown in Equation (1):

(1)

where

= (2)

DTW aims to find the warping path $W = \{w_1, w_2, \ldots, w_k, \ldots, w_K\}$ of contiguous elements on the distance matrix such that $\max(n, m) < K < m + n - 1$, and $w_k =$, thereby minimizing the value calculated via Equation (3), as smaller total path distances indicate better alignment between datasets:

(3)

The warping path that defines the alignment between two time series matrices is subject to the following constraints [4]:

- It must start and finish in diagonally opposite corner cells of the matrix.
- The steps in it are restricted to adjacent cells.
- The points in it must be monotonically spaced in time.

Theoretically, it would be ideal to include all measured variables and corresponding monitored variables into the model, but the resulting computational time would be unfeasible. Therefore, an engineering assessment was employed to select specific variables, values of which were used in a sensitivity analysis on an input parameter of interest (PV-006 opening). The selection also depends on the primary goals of the desired validation analysis.

3. EXPERIMENTAL DATA ANALYSIS

The original experiment plan was submitted to the DETAIL operating team so they could generate data providing more insight into the TEDS performance. The experiment plan corresponded to simulated operation from an initial modeling run. However, the actual operation plan ultimately deviated from the submitted plan due to certain unanticipated conditions observed during the experiment. This is not unexpected as the TEDS system has effectively just passed commissioning (delayed by operation accident in 2021) and there is limited operation experience and data.

3.1 Experiment Plan

The experiments were based around the TEDS system. After restarting and recommissioning this system, an experimental procedure was proposed for verifying the system parameters and operation. This experimental procedure was partly modified both before and during the experiment, due to certain newly identified limits imposed on the system (discussed later). The main focus was the thermocline tank, with the specific points of interest being the experimental temperature stratification during charging, discharging, and standby storage. The temperature stratification during standby storage was of particular interest in terms of observing the extent of residual heat transfer between stationary oil and the alumina packed bed beads. However, other operating regimes were also explored (e.g., heater to load). The original experimental plan can be summarized as follows.

- Start oil circulation, bypassing the glycol HX; heat the oil to 300°C.
- Start charging.
  - Admit the oil to pass through the packed bed storage tank.
  - Keep the circulation rate constant to maintain a steady oil temperature of 300°C at the heater outlet.
  - Charge until the thermal front (260–295°C) reaches about two-thirds of the tank height.
- Stop charging, switch to load mode.
  - Run in heating mode but bypass the TES; reject heat via the glycol HX.
  - Maintain heating mode for 30 minutes.
- Start discharging.
  - Set the flowrate identical as the charging flowrate, identified during the charging operation.

- Adjust the valves for controlling the flow through the glycol HX in order to maintain an oil temperature equal to 100°C at the outlet of the glycol HX.
- Discharge until the thermal front (140°C) drops back down to about a third or a fourth of the tank height.

- Shut down the oil pump for at least 30 minutes before cooling and shutting down the TEDS loop (i.e., cooling to a walk-away safe temperature, then shutting down the pump).

This plan was known to be aggressive, knowingly put in place to explore some of the limits of the system. Therefore, after newly identifying system limits, certain setpoint values had to be adjusted. This included only a limited capability of reducing the oil flowrate (the variable-frequency drive was operating at 7 Hz) when seeking to maintain hot oil temperature at 300°C. Maximum heat rejection was observed at the glycol HX that prevented reaching the desired outlet oil temperature. Also, the positions of the multipoint thermocouples were found to be opposite of what is seen in the previously established thermocouple map (centerline vs. wall). Some of these limitations were only discovered during operation, but can be well managed in future experiments, e.g. also throttling valves, not only reducing pump speed, to maintain control at low flowrates. Thus, the experimental plan for the as-performed experiment (including all modifications) can be summarized as follows (main modifications in bold):

- Start oil circulation, bypassing the glycol HX; heat the oil to 300°C.
- Start charging.
  - Admit the oil to pass through the packed bed storage tank.
  - **Gradually adjust** circulation rate to achieve a **constant oil temperature at the heater outlet at maximum power, a suitable setpoint found to be 250°C for a pump speed of 7 Hz.**
  - Charge until the thermal front (**210-245°C**) reaches about two-thirds of the tank height.
- Stop charging, switch to load mode.
  - Run in heating mode but bypass TES; reject heat via the glycol HX.
  - Maintain this regime for 30 minutes.
- Start discharging.
  - Implement the same pump speed as was used for charging.
  - Adjust the valves controlling the flow through the glycol HX to achieve an oil temperature of 138°C at the glycol HX outlet (i.e., the minimum temperature achievable at the beginning of discharge when there is zero bypass of the glycol HX).
  - Discharge until the thermal front (170°C) drops back down to about a fourth of the tank height.
- Switch the system into bypass mode (no flow through storage, heater off) for at least 30 minutes before cooling and shutting down the TEDS loop (i.e., cooling to a walk-away safe temperature with nominal flowrate via heat rejection through the glycol HX, then shutting down the pump).

The experimental plan was also implemented in the Modelica model. Figure 4 shows the model's predictions of some of the main parameters, such as tank stratification temperature, temperature within the cycle, and heater power or oil flowrate. Note that the model generated these predictions prior to integrating the updated timetable-based control system.

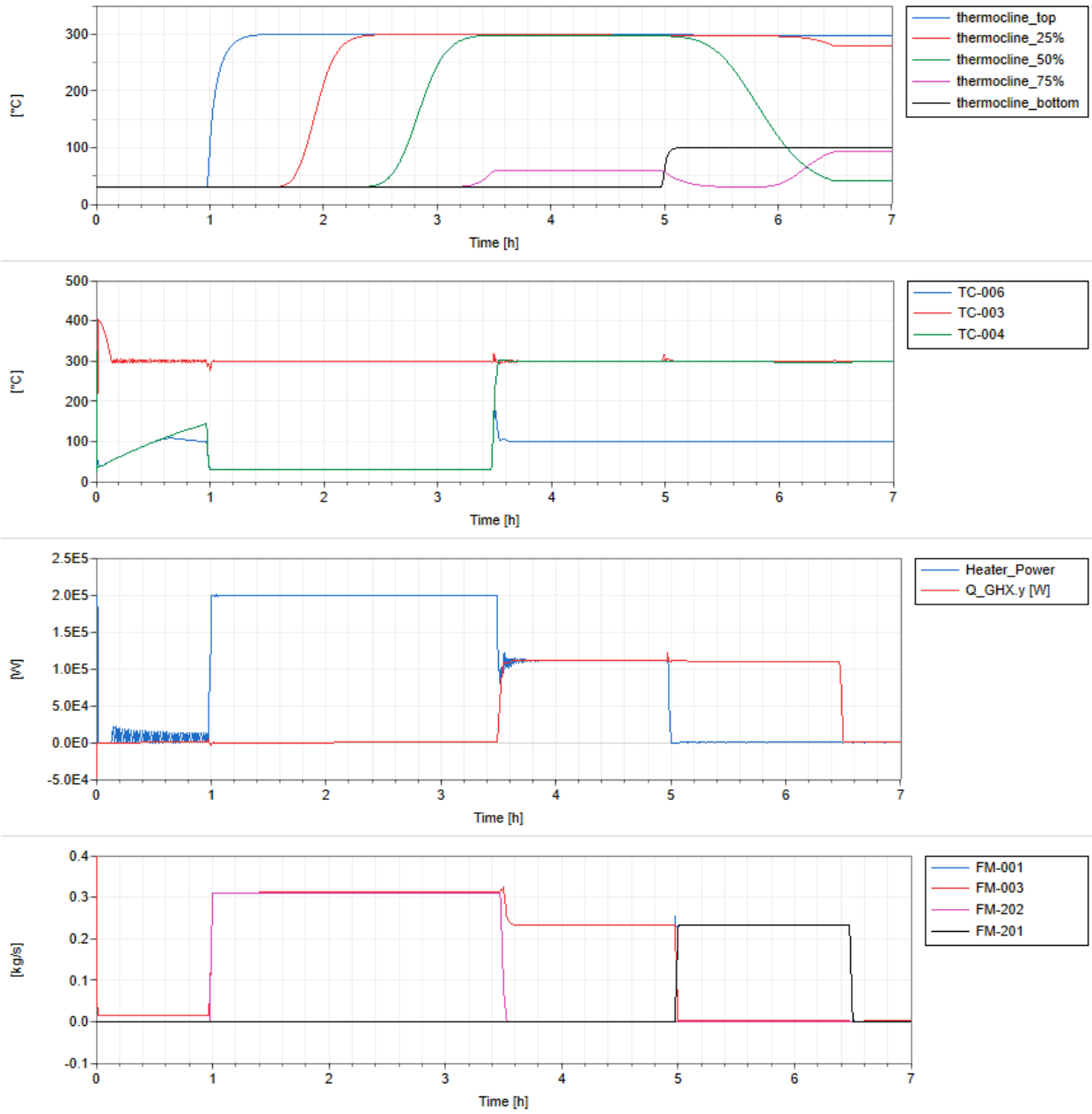

Figure 4. Expected system parameters, as predicted by the Modelica model.

3.2 Initial Experimental Data Analysis

The data were analyzed in regard to general behavior and eventual anomalies. Due to a lack of clarity on certain points, previous data from 2021 were also revisited. When referred to specific sensor or actuator, please see Appendix A for the TES P&ID, a drawing of the thermocline tank, and a map of the thermocouples within the tank.

3.2.1 System parameters

The main values of interest were the temperatures throughout the system, the temperatures within the thermocline, and the flowrates, as presented in Figure 5, Figure 6, and Figure 7, respectively. The thermal load of the heater (calculated from oil data, the electrical power was not recorded) was then calculated

from the experimental data, as presented in Figure 8. To more easily distinguish among the different operating regimes, vertical lines have been added to mark the transition points. Note that flowrates through most of the flowmeters turned out to be below the range of effective measurement. The thermal load of the glycol HX was calculated using flowmeter FM-002, which was, however, unreliable. Therefore, a second, adjusted value was obtained using the overall flowrate from sensor FM-001, which provided valid readings throughout the entire operation, along with the difference between the HX inlet temperature (TC-004) and the temperature after mixing with the bypass line (TC-006).

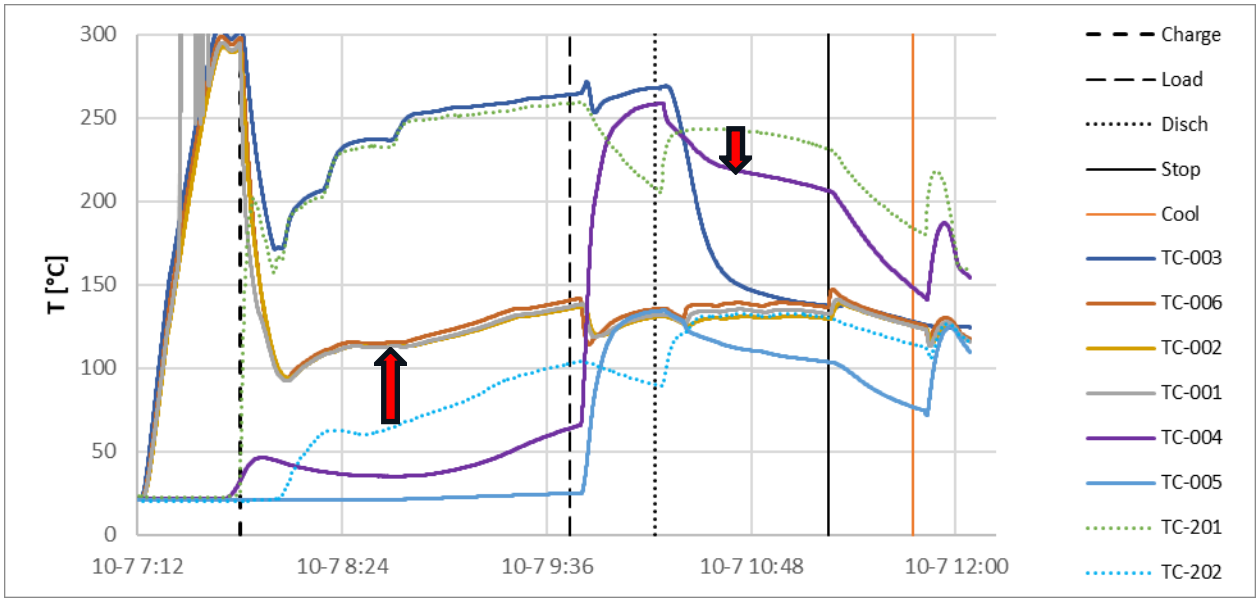

Figure 5. Recording of temperatures within the system, generated from the experimental test. Red arrows highlight anomalies in the temperature profile, as explained in the text.

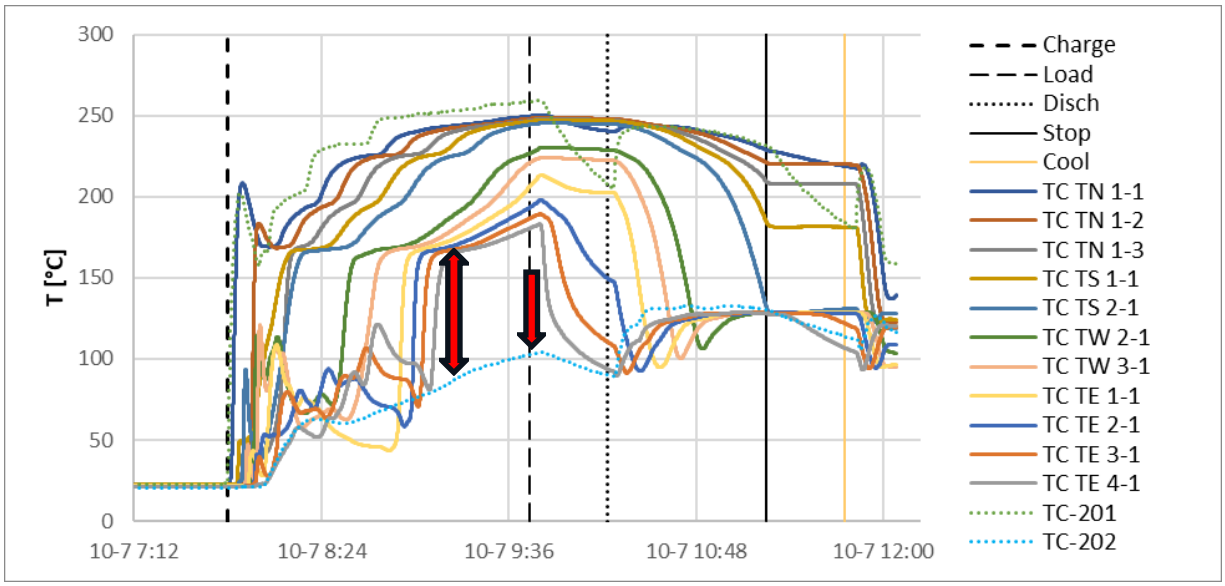

Figure 6. Recording of temperatures within the thermocline tank, generated from the experimental test. Red arrows highlight anomalies in the temperature profile, as explained in the text.

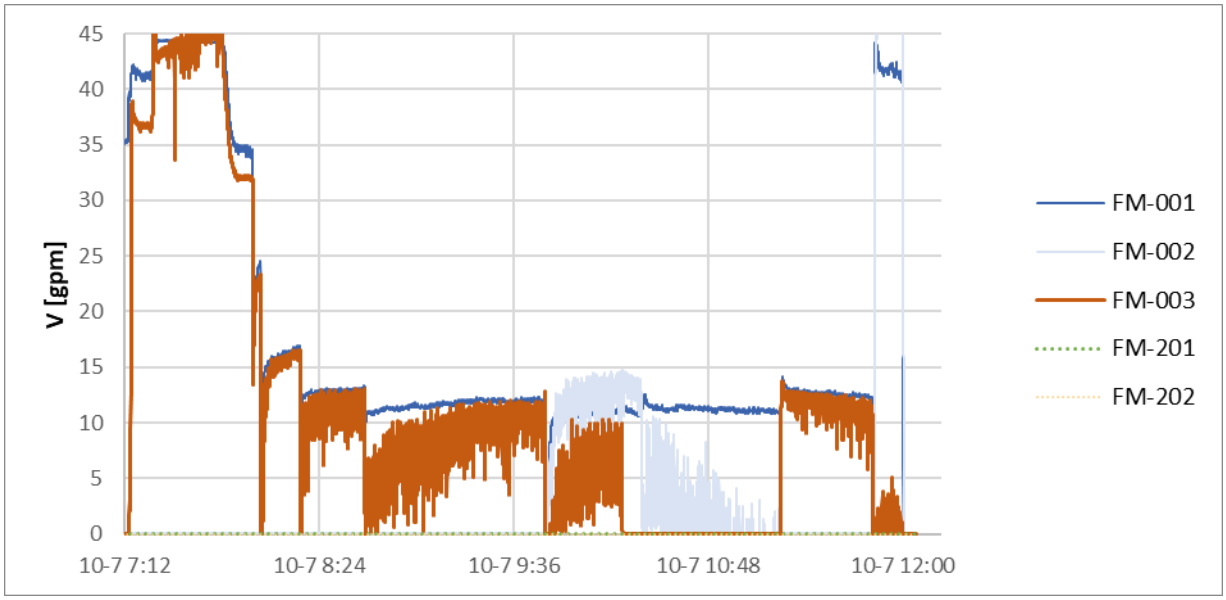

Figure 7. Recording of flowrates within the system, generated from the experimental test.

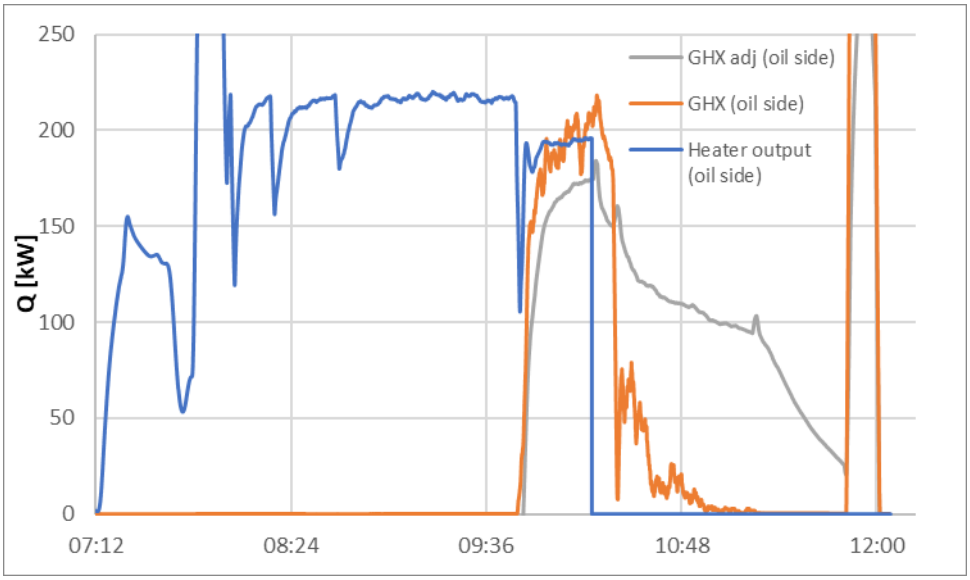

Figure 8. Calculated duties of the heater and glycol HX in the experimental test.

In looking at the experimental data, several anomalies were observed, as highlighted by the arrows in the figures above. First, during charging, a temperature increase is seen between the thermocline tank cold outlet (TC-202) and the downstream temperatures before and after the pump and before the heater (TC-006, TC-001, and TC-002, respectively). During discharging, a relatively large temperature drop occurs between the thermocline tank hot outlet (TC-201) and the downstream temperature at the inlet of the heat-rejecting glycol HX (TC-004). This temperature drop is rather high to correspond only of the thermal losses.

A hypothesis to explain this behavior—as there is no heat source other than the heater—is that the increased temperature could be caused by a leaking valve (PV-006), thus mixing the cold tank outlet with the hot oil. This would also explain the high temperature drop of TC-006 during discharging, where, on the other hand, the cold oil mixes with the tank hot outlet. A similar temperature profile was observed in a

single dataset from 2021, yet not in any other, further suggesting the random nature of the occasional improper valve closing.

After stating this hypothesis and also confirming the valve leak by using a model (as described below), a new experimental test was planned and performed, specifically focusing on validating the improper closure of this valve. The test confirmed this behavior, and system adjustments to fix the valve need to be made.

The next anomaly can be observed in temperature profiles within the thermocline tank. During charging, the bottom temperatures exhibit a steep rise, with the bottommost temperature, TE 4-1, exhibiting this behavior at around 9:07. It could be deduced either that the tank is charged or that a flow (thermal) breakthrough—defined as the temperature of the thermal front reaching the bottom of the tank without charging the whole tank—has occurred and that the outlet temperature, TC-202, should soon follow. However, neither of the cases reflect reality as the temperature TC-202 rises only gradually and maintains significant difference from TC TE 4-1. Following up on this, after the charging is stopped at 9:44, the bottom thermocline temperatures drop very quickly, despite there being no flow. A certain drop in temperature was expected as a result of temperature equilibration between the oil and the packing material (beads), due to the heat transfer limitations (heat transfer coefficient, Biot number). Still, this does not explain why the hot oil does not break through even after a prolonged period, since the bottommost temperature jumps up. The temperature equilibration is significantly lower during discharging, even near the thermal front, where a temperature rise of only 3K was measured for TS 2-1. In comparison, the bottommost temperature (TE 4-1) fell by almost 90K in the standstill period after charging. (Note that some of that temperature drop could also be due to thermal losses. During the standstill period after discharging, the temperature measured by TE 4-1 drops by about 20K.) Part of the explanation for what is happening may be a potential flow channeling, with radial equilibration being seen in the radial temperature profiles (see next section 3.2.2). Still, the question of why the hotter oil does not appear at the outlet remains unanswered, unless perhaps this temperature reading is incorrect.

3.2.2 Thermocline spatial temperature profiles

The radial and axial temperature profiles in the thermocline tank were also explored within specified time periods (i.e., shortly after the start of charging, in the middle of charging, at the end of charging, near the end of the standstill period after charging, and before the end of discharging). The specific times are listed below. One-minute averages were calculated within each time period. Several (not centerline) temperature probes were reading incorrect values. If such values were between two correctly read temperatures at the same radius, the averages of the above and below temperatures were used for the graphic representations of the temperature profiles below. In the profile, the inlet and outlet temperatures are also included as the first and last values. For the thermocouple locations, please see Appendix A, which includes a drawing of the thermocline tank and a map of the thermocouples within.

- Start 8:00
- Mid charge 8:50
- Charged 9:44
- Hold 10:13
- Discharged 11:13

First, Figure 9 shows the centerline profiles at the listed times. Note the rather erratic temperature profile during charging, especially soon after the charging begins. This can be partly caused by the manipulation and adjustments of the flowrate, as the nominal temperature was not reached for a notable amount of time because the flowrate was too high. Some aspects of the profile may be the result of the flow channeling prematurely increasing the outlet temperature. This highly contrasts with the discharge profile, which shows a very smooth temperature profile in the bottom of the tank, in addition to a visible thermal front—though still not very sharp—on top of which remains close-to-charged temperature. At the end of charging, a gradual temperature profile in the bottom is seen to end at 180°C, while the outlet is

only around 100°C. Slightly more as-expected stratification is obtained from the measurement taken after the standstill period. The difference between these temperatures was referred to in the previous section 3.2.1 as an unclear anomaly. Note that the bottom of the tank, which is the outlet during charging, would ideally remain at a constant initial temperature.

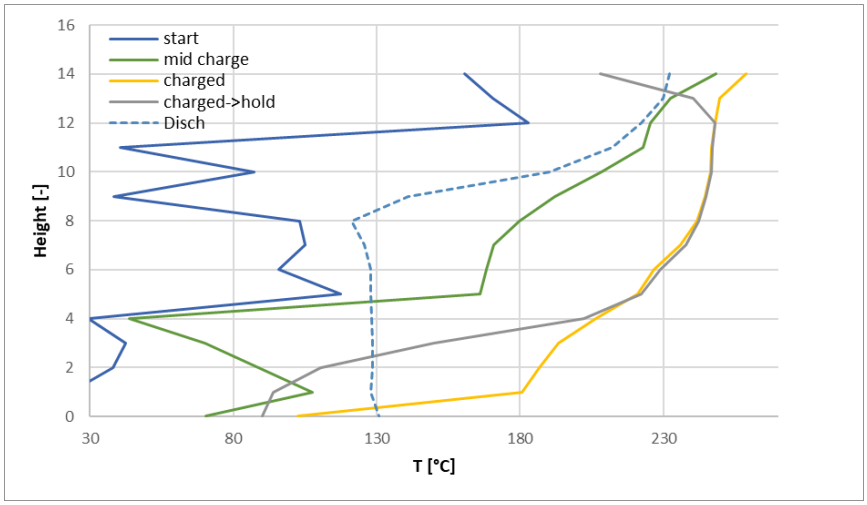

Figure 9. Centerline temperature profiles in the tank, for all times considered.

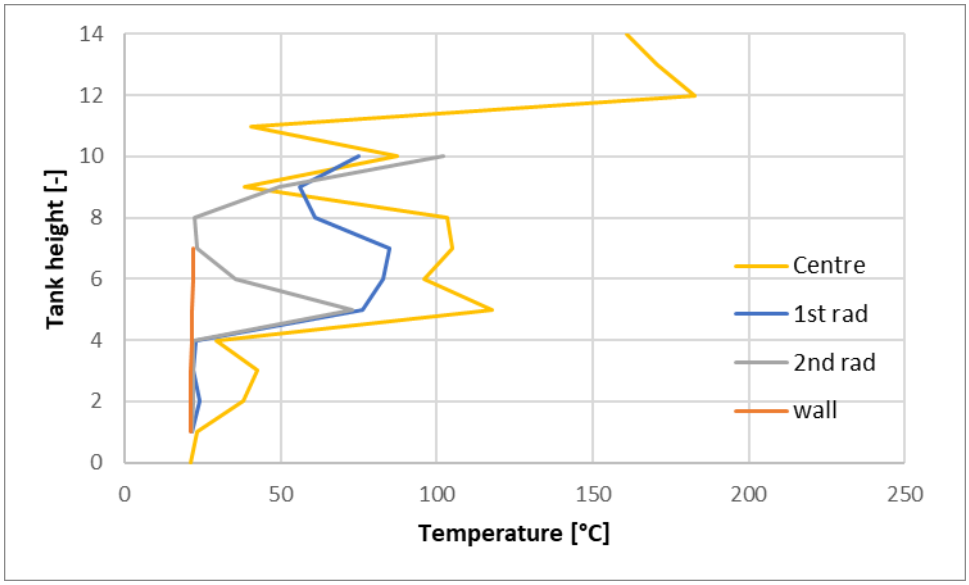

Figure 10. Temperature distribution within the thermocline tank, based on the available radial positions at a specific time soon after the charging was initiated.

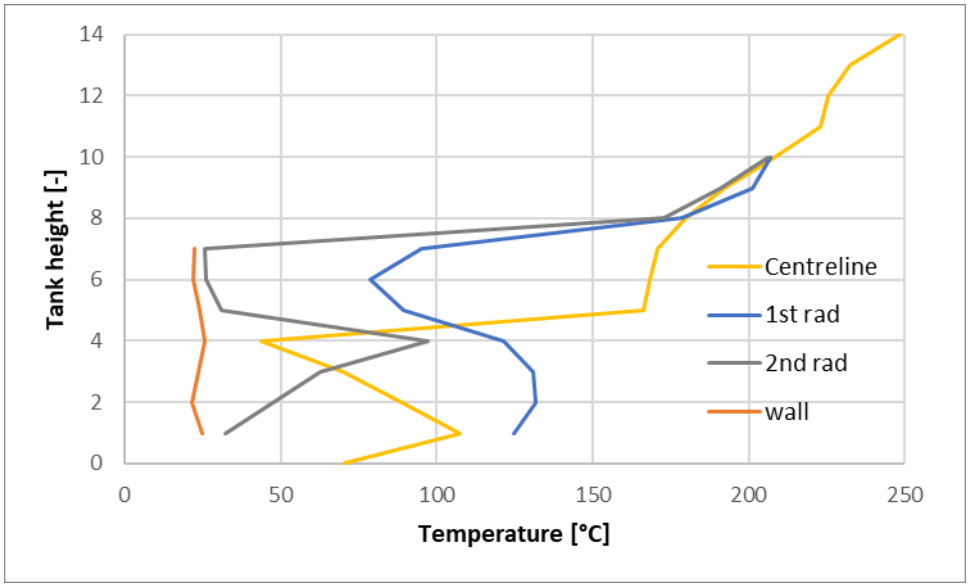

Figure 11. Temperature distribution within the thermocline tank, based on the available radial positions at a specific time in the middle of the charging process.

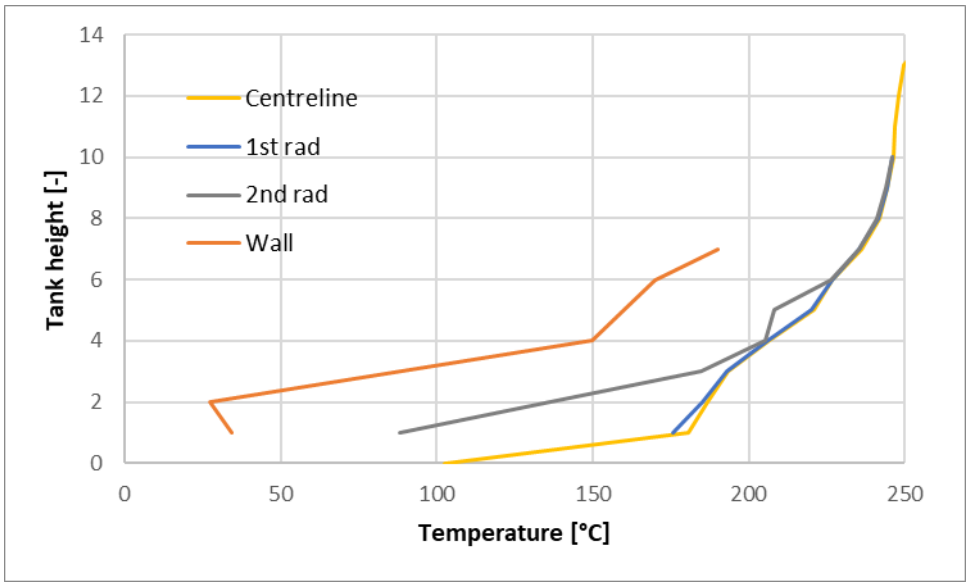

Figure 12. Temperature distribution within the thermocline tank, based on the available radial positions at a specific time at the end of the charging process.

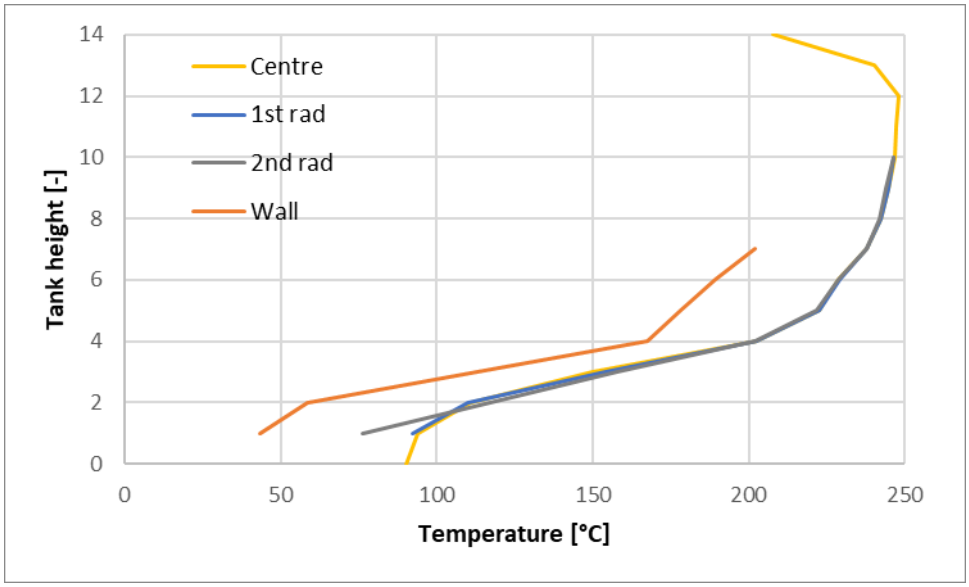

Figure 13. Temperature distribution within the thermocline tank, based on the available radial positions at a specific time at the end of the standstill period between charging and discharging.

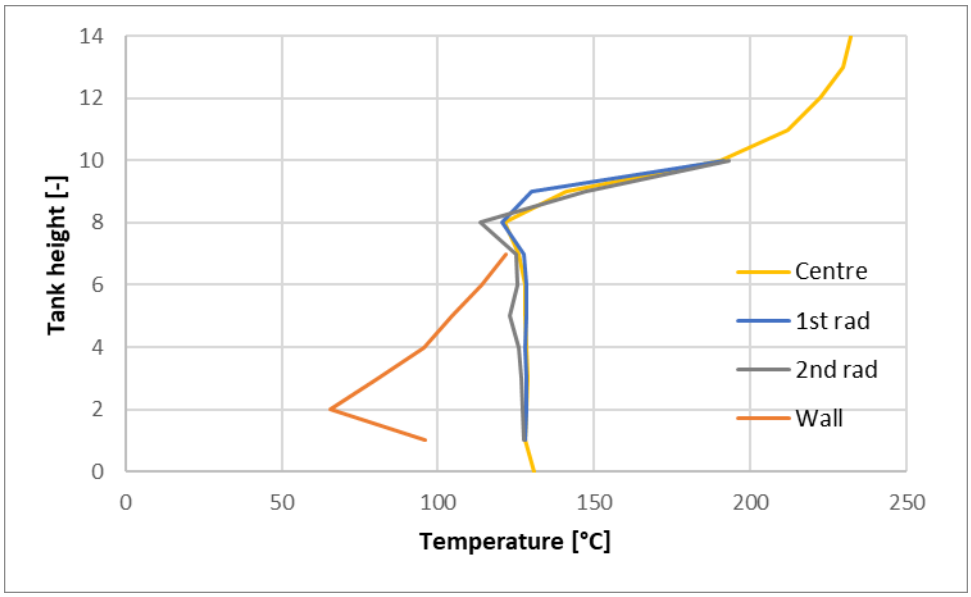

Figure 14. Temperature distribution within the thermocline tank, based on the available radial positions at a specific time at the end of the discharging process.

4. VALIDATION AND ADJUSTMENTS OF THE MODELS' NOMINAL PERFORMANCE

4.1 Glycol Heat Exchanger

The capabilities of the validation code were demonstrated by fitting the parameters of an HX with an unknown internal configuration to match the nominal conditions listed in Table 1. Here, the HX was a helical coil type that utilized hot thermal oil on the tube side and a cold glycol-water solution on the shell side (see Figure 15). This HX was delivered by a vendor to match the nominal specified parameters, but documentation on the internal specific configuration remains proprietary to the vendor.

A simple model featuring only the HX and boundary conditions was assembled, as shown in Figure 16. The HX was tested by using mass-flow-source components to supply primary and secondary fluids at a specified mass flow rate and temperature. The HX test pressures were specified at the primary and secondary fluid exits, using pressure boundary components. The HX's nominal parameters are summarized in Table 1, with the first two rows corresponding to the inputs for the sources.

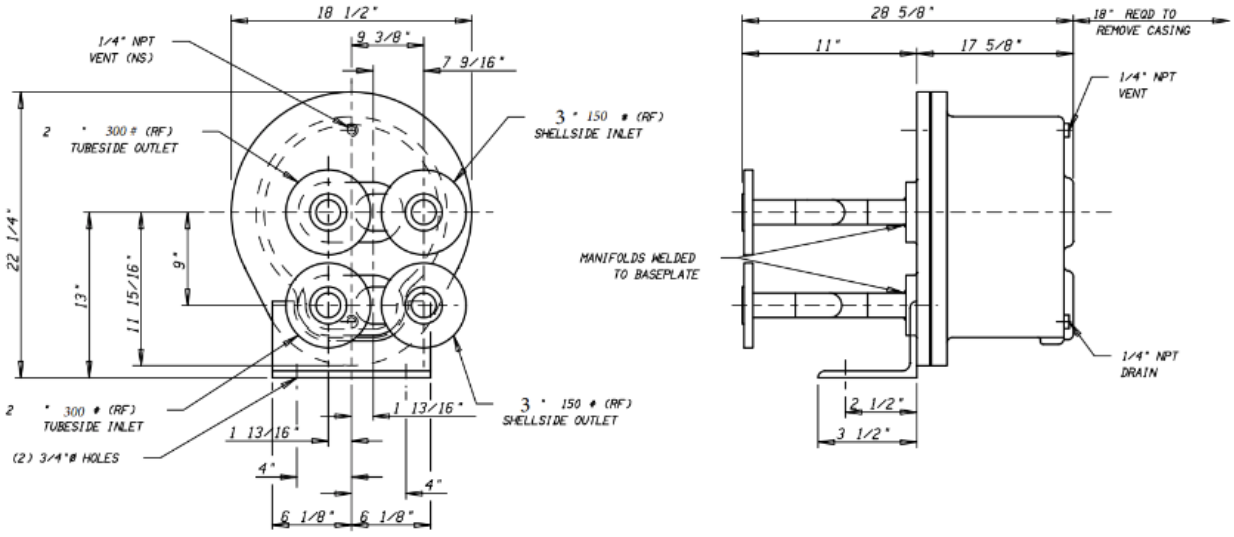

Figure 15. Manufacturer-provided drawing of the HX.

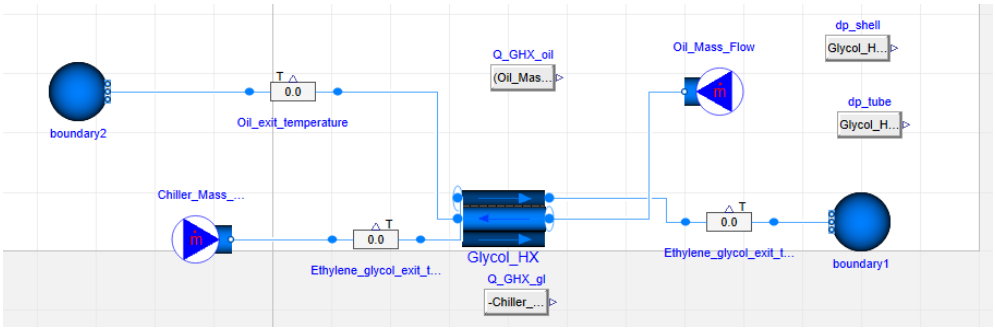

Figure 16. Simple glycol HX model with boundary conditions.

Complex optimizer tools were not needed, as this type of validation task can be well-performed using Dymola's parameter sweep function. This function was run to match unknown parameters —specifically, the tube length and diameter—to the design performance, while keeping several parameters that had been estimated based on available drawings and manufacturers' specifications. Table 2 summarizes the resulting parameters for this case. Some discrepancies pertaining to surface area likely stem from

uncertainty in the heat transfer correlations (especially for a helically wound HX) when the baseline model represents a standard shell-and-tube HX, as well as from the manufacturer's safety margins for somewhat atypical working fluids. The manufacturer-specified pressure drops should include all minor losses from any entrances, exits, bends, internal baffles for directing flow, etc.

Table 1. Nominal HX parameters.

	Tube-side	Shell-side	Unit
	Therminol® oil	eth. glycol solution	
Mass flowrate	1.74	12.44	kg/s
Inlet T	325	6.67	°C
Outlet T	220	17.78	°C
Pressure drop	10.1	61.8	kPa

Table 2. Tuned HX parameters for achieving the specified oil outlet temperature.

	Manuf. Specs	Tuned / set	Unit
Heat transfer rate	455	440	kW
Surface area	4.54	3.45	m^2
Shell D (outer / inner)	0.47 / n.a.	n.a. / 0.44	m
Shell length (outer / inner)	0.44 / n.a.	n.a. / 0.37	m
Tube D	n.a.	50 x 1.5	mm
Tube length	n.a.	22.0	m
n tubes	n.a.	1	-
Pressure drop shell	61.8	0.3	kPa
Pressure drop tube	10.1	5.8	kPa

4.2 Thermocline Tank

For the thermocline tank it was found already during the initial analysis of the experimental data, that some phenomenon as flow channeling is taking place, causing significant discrepancy from model behavior. Flow channeling cannot be accounted for in the model as only axial discretization is applied [4]. Rather than performing analytical validation of the model, more experiments should be performed to identify if different operating conditions can mitigate this adverse effect. Looking at Figure 11-Figure 14, the impacts of apparent channeling appear to be more pronounced during charging than during discharging. It is possible that lower flowrates or a smaller temperature difference between charged and discharged tank may also reduce the radial temperature gradients. Future testing should analyze this.

The flow rates required to match the experimental plan in this case were sufficiently low so that they were outside the range of the flowmeters in the system. The improperly closing valve contributed to this by splitting flow unexpectedly. Operating experiments with smaller temperature delta setpoints may drive the system to operate where the flowmeters can accurately measure.

It is still possible to replicate the full system operation within the model, and thus computationally determine flowrates even when the flowmeters do not properly measure conditions. Therefore, in this work, validation of the thermocline tank is not performed separately. Rather, it is considered a component of TEDS being validated in its entirety. Through this holistic validation, component validation of the thermocline is complete.

5. MODEL VALIDATION FOR DYNAMIC OPERATIONS

5.1 Modelica Model Setup

Based on the actual experiment operation, valve positions and other inputs for the required operating regimes (illustrated in Section 3.1) are dictated into the Modelica model via parameterized sequences using a Modelica 'timetable' block. These sequences are presented in Figure 17. The valves are considered open at a value of 1 and closed at a value of 0. This sequence assumes that PV-006 never fully closes. Note that, in specific operating modes, the modelling measurements equivalent to TC-003 and TC-006 shown in Figure 17 are off the scope in order to ensure that the heater is off or that the glycol HX is being bypassed, as needed. This is a modeling artifact of Modelica, and the off the scope measurements should be ignored.

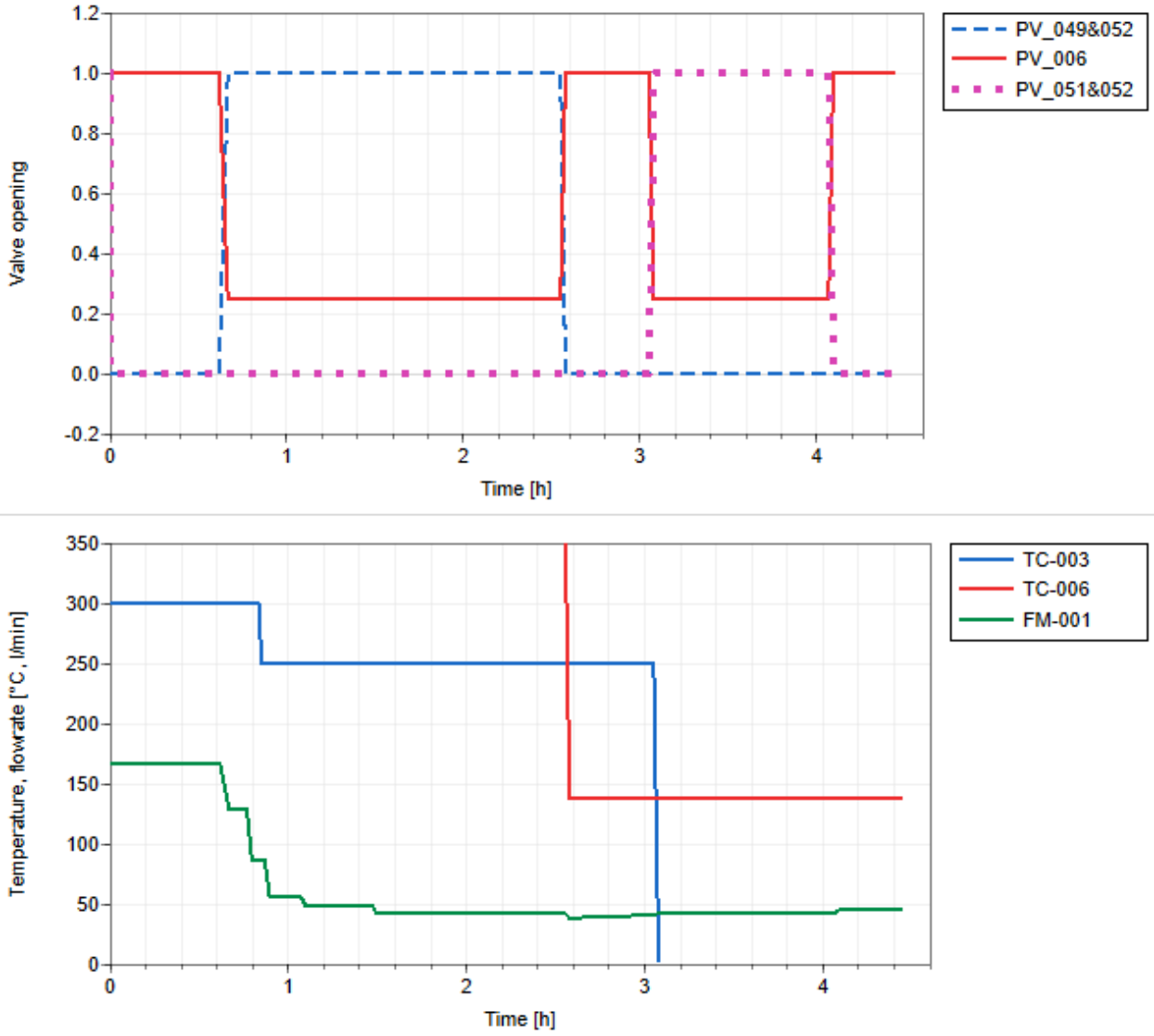

Figure 17. Input sequences of valve-opening, temperature, and flowrate setpoints.

Figure 18 presents the main simulation results for the case involving an assumed leaky valve (PV-006), whereas Figure 19 corresponds to the case in which PV-006 closes properly. Note that in the simulation in which PV-006 closed properly, the thermal front first passed through the tank at low

temperature, resulting in temperature oscillations and, briefly, insufficient power to maintain the heater setpoint temperature. In addition, the thermocline tank did not properly charge at the (new) nominal temperature of around 250°C. As the tank was insufficiently charged, it could only maintain the discharging temperature for a short period after discharging commenced. The temperature drop at the location of TC-202 was also slower in this case.

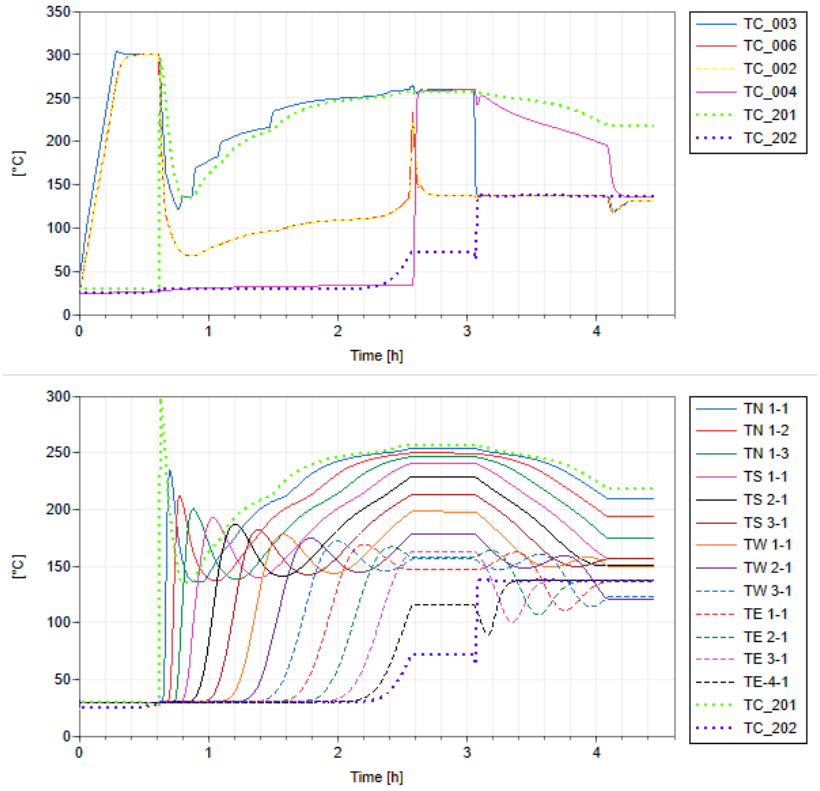

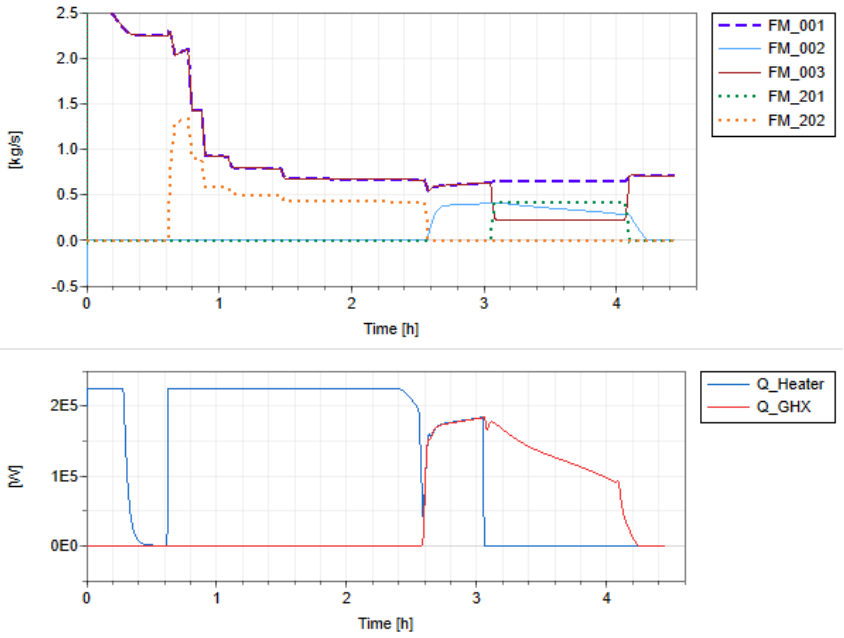

Figure 18. Simulation results parameters when assuming that the leaky valve (PV-006) remained 25% open instead of fully closing.

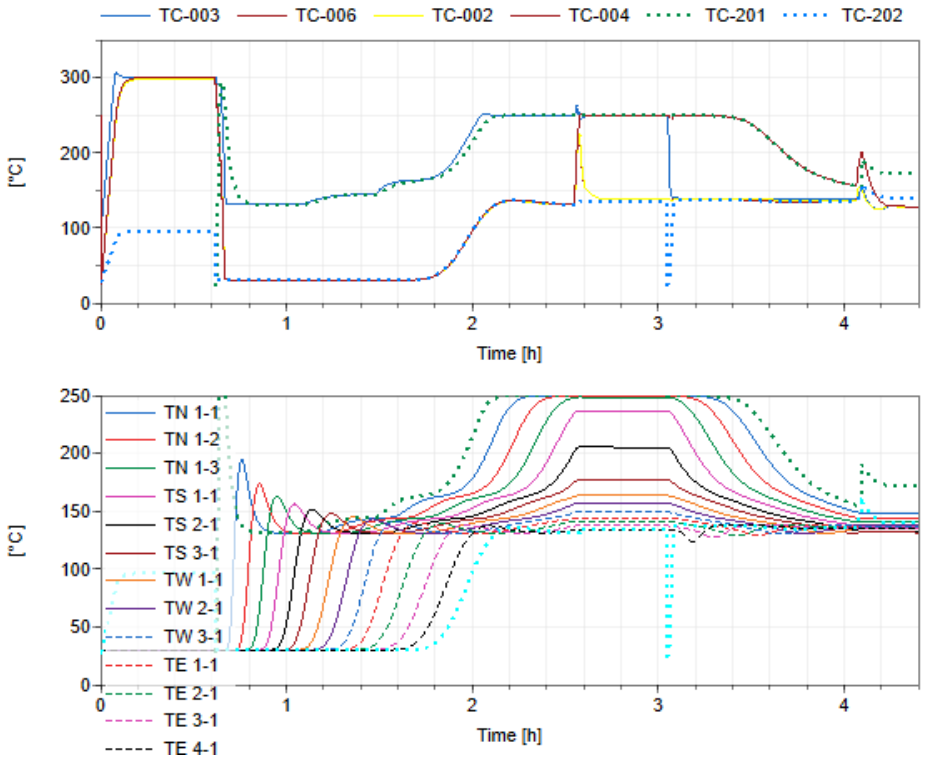

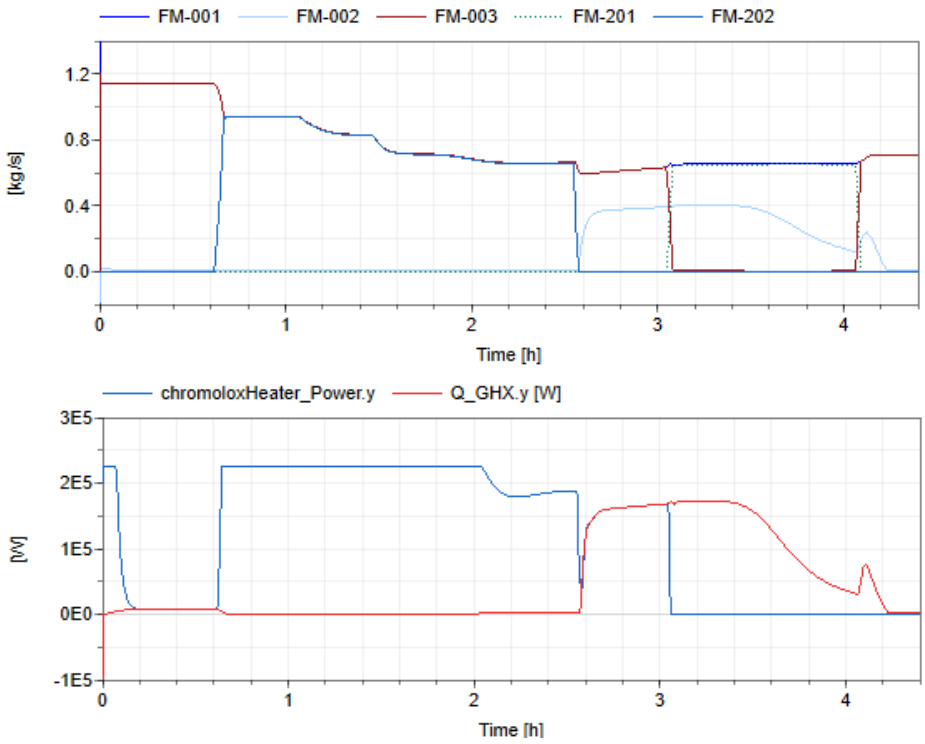

Figure 19. Simulation results parameters when assuming that the valve (PV-006) closed properly.

5.2 Preliminary Analysis

Before performing the DTW calculation and validating the simulation data against the experiment data, visual comparison of a selected parameter (i.e., TC TN 1-2) was performed (see Figure 20). In addition to the single experiment result (i.e., reference time series) were the following four simulation model results (i.e., query time series):

- PV-006 fully closes (valve area = 0.0)
- PV-006 is a quarter of the way open (valve area = 0.25)
- PV-006 opens halfway (valve area = 0.50)
- PV-006 fully opens (valve area =1.0).

Simple visual comparison reveals that temperature profiles based on a partially opened valve more closely align with the experiment data than do the ones based on fully closed or fully opened valves. A better fit is seen for “25% open” during charging and for “50% open” during discharging. This phenomenon possibly signals a different pressure drop distribution in each branch of the thermal oil, where it can flow within the TEDS. There is different ratio of the pressure drop between each branch for each regime of operation. The flow would naturally distribute itself to different branches based on their pressure drops. The same valve opening during various regimes can thus result in different flowrate distributions through the respective branches, especially as the pressure drop equation used within the valve is different from the anticipated pressure drop equation that would more accurately describe the physics of the situation. As valves are typically controlled, this is not seen as an issue during normal operation.

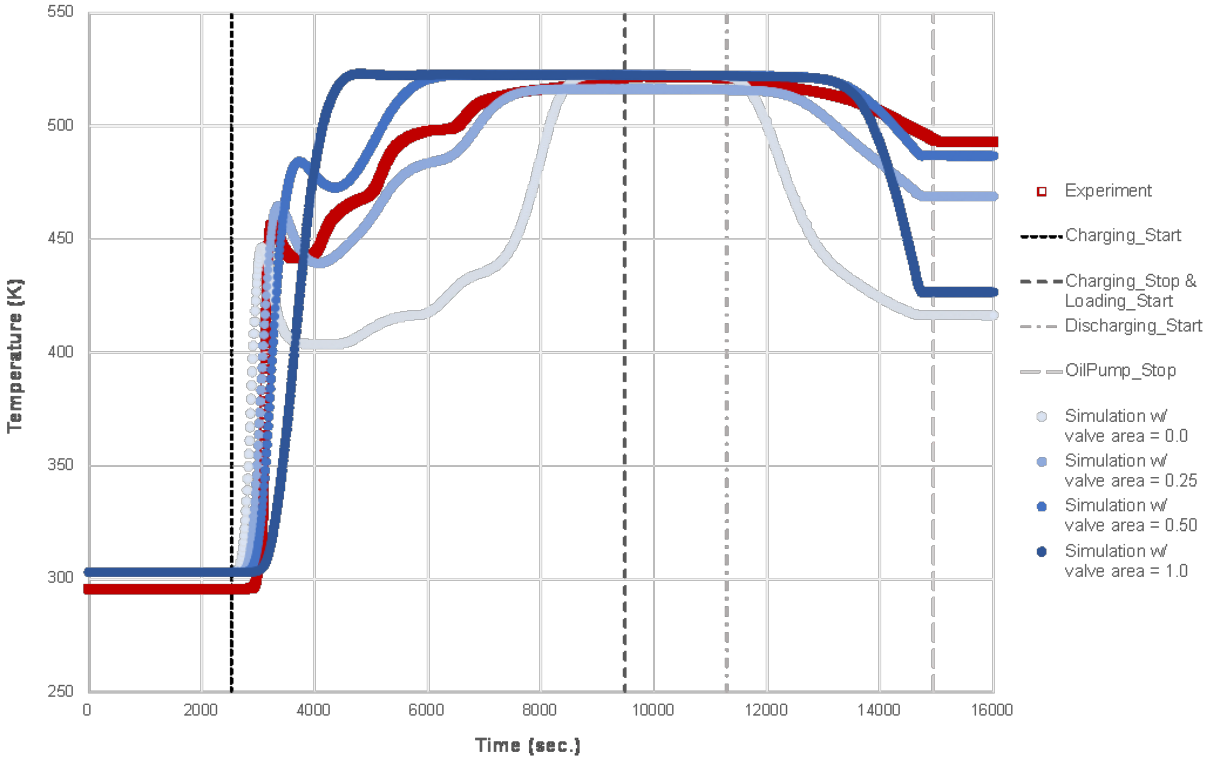

Figure 20. Temperature profile of thermocouple TC TN_1-2 in the thermocline tank, and its corresponding variable in the Modelica model (thermocline_Insulation.thermocline_fluidprops_heaters_newHC_120C.Tf[28]).

5.3 Model Adjustment with Parameter Fitting

To demonstrate the model validation approach, a series of simulations were used to model the PV-006 valve opening over a value range of 0.0–1.0. For each simulation, the DTW distance for a single pair of temperature profiles (i.e., experiment vs. simulation) was calculated. The DTW distance graphs for the single parameter, TC TN 1-2 (y-axis value, in Kelvin), with respect to the PV-006 opening area are plotted in Figure 21. The x- and y-axes in each subplot in Figure 21 represent the time index (1 index = 300 seconds) and temperature, respectively. A good match is seen during the initial bypass, but once PV-006 is required to close and the system begins to charge, the gap between the simulation and the experimental data begins to widen. One sees significantly better matching for the models that feature the valve partly open, with the DTW distance reducing from 1451 for fully closed to 308 for 40% open. The remaining discrepancy between the modelling and experimental results can be largely attributed to unanticipated flow channeling within the thermocline storage—something for which the model does not account, as has been discussed. It is worth noting that any deviation of the modelling results is reduced as the opening area of PV-006 increases from 0% (fully closed) to 40% (i.e., the lowest DTW distance). When PV-006 is 30-40% open, this seemingly produces the closest agreement with the experimental values. Once the valve opening area exceeds 40%, the discrepancy grows because the temperature profile of the simulation data during the charging mode reaches charged temperature faster than in experiment. This is caused by the increased return temperature after mixing, raising the heater inlet temperature and shortening the time before the heater power is sufficient to achieve the setpoint temperature. In each subplot of Figure 21, the dotted line connecting two different time series means that they are the two closest matching points in those series. In addition, note that the amount of discrepancy between two time series is dependent on the operating mode. The discrepancy between two time series during discharge

mode (see also Figure 20) is minimized when the valve opening area reaches around 40% while for charging there is better agreement when the valve opening is around 30%. The valve equation in the model is linear (pressure drop, mass flow, and opening area are all linearly related), as a linear model can more efficiently simulate the fact that controlled valves can typically be precisely opened to manage flowrates as needed. A stuck-open valve would lead to an opening (orifice) in which the pressure differential would scale with mass flowrate to the second power. Also, each branch of thermal oil flow, separate for charging and for discharging, has not been precisely tuned for their pressure drop. Thus, as the actual system pressure distribution changes, the stuck-open valve does not precisely account for the pressure drop. Accordingly, the flowrate distribution will also differ. This indicates there should be multiple input variables to calibrate the temperature profiles. The purpose of the present work is to confirm the hypothesis behind the aforementioned (potential) system fault so that it can be fixed, not to precisely fine-tune parameters so that they correspond to this faulty regime. DTW distance graphs for other variables are given in Appendix B.

Multivariate DTW distance for additional temperature sensors in the system were calculated so that the discrepancy between the simulation and the experiment data becomes reduced over the system in general. The selected temperature points[a] are:

- 3 temperature points along the thermocline height: TN-1-2, TS-1-1, and TW-3-1
- 4 temperature points within the system: TC-201, TC-202, TC-006, and TC-004.

The resulting DTW maps for selected variables are shown in Figure B-1 through Figure B-6 and for overall variables are shown in Figure 22. In Figure 22, the colors in each subplot represents the DTW distance between two datasets. The x- and y-axes represent the time index (1 time index = 300 seconds) for the query (simulation) and the reference (experiment) data, respectively. The red line in each plot represents the optimal warping path. The line is closest to diagonal is seen for opening around 30%, meaning the best match without considering time delays between time series. The colors of shortest distance are less visible except for the high deviations from the optimal valve opening. When the DTW was applied for all seven of the considered parameters listed above, this optimization routine determined the optimal value to be around 20%. For further clarity, Figure 23 shows the combined DTW distance with respect to the PV-006 opening area.

Overall, good agreement is observed between the modelling data and experimental data. The TEDS model is considered to be preliminarily validated, with the understanding that future work may be able to further improve the accuracy of the model in predicting the physical state of the system. Additionally, through the existence of the model, the operation of the physical system may be able to be safely extended beyond the measurement ranges of the temperature and flow meters in the system. The model is shown to be accurate and can be used as a surrogate for the physical measurements where needed.

[a] For the thermocouple locations, please see Appendix A for the TES P&ID diagram, a drawing of the thermocline tank, and a map of the thermocouples within.

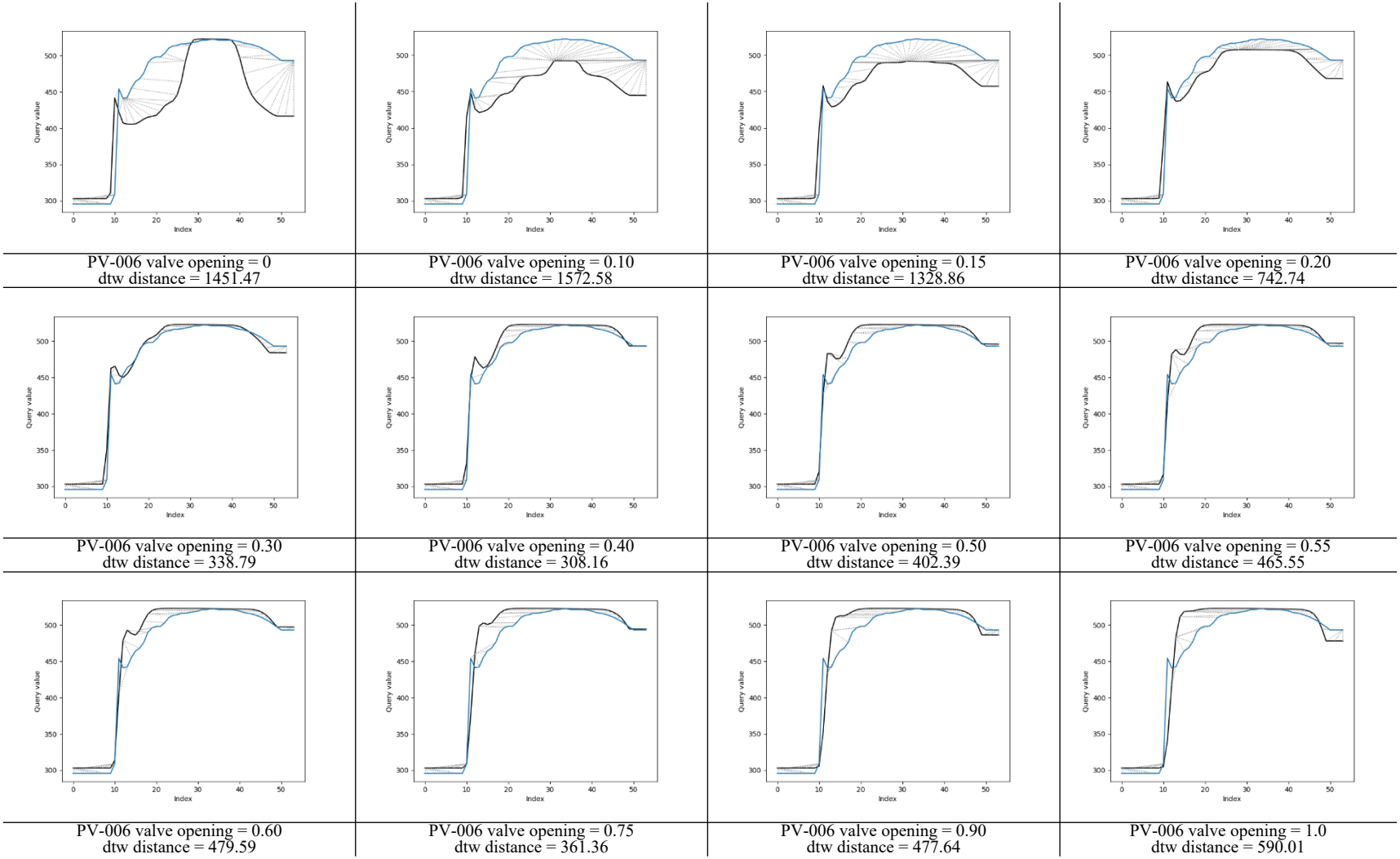

Figure 21. DTW distance between the simulation data (i.e., solid black line) and the experimental data (solid blue line) in regard to the thermocline temperature at the target location (i.e., TC TN 1-2). The x- and y- axes in each subplot represent the time index (1 index = 300 seconds) and temperature (K), respectively.

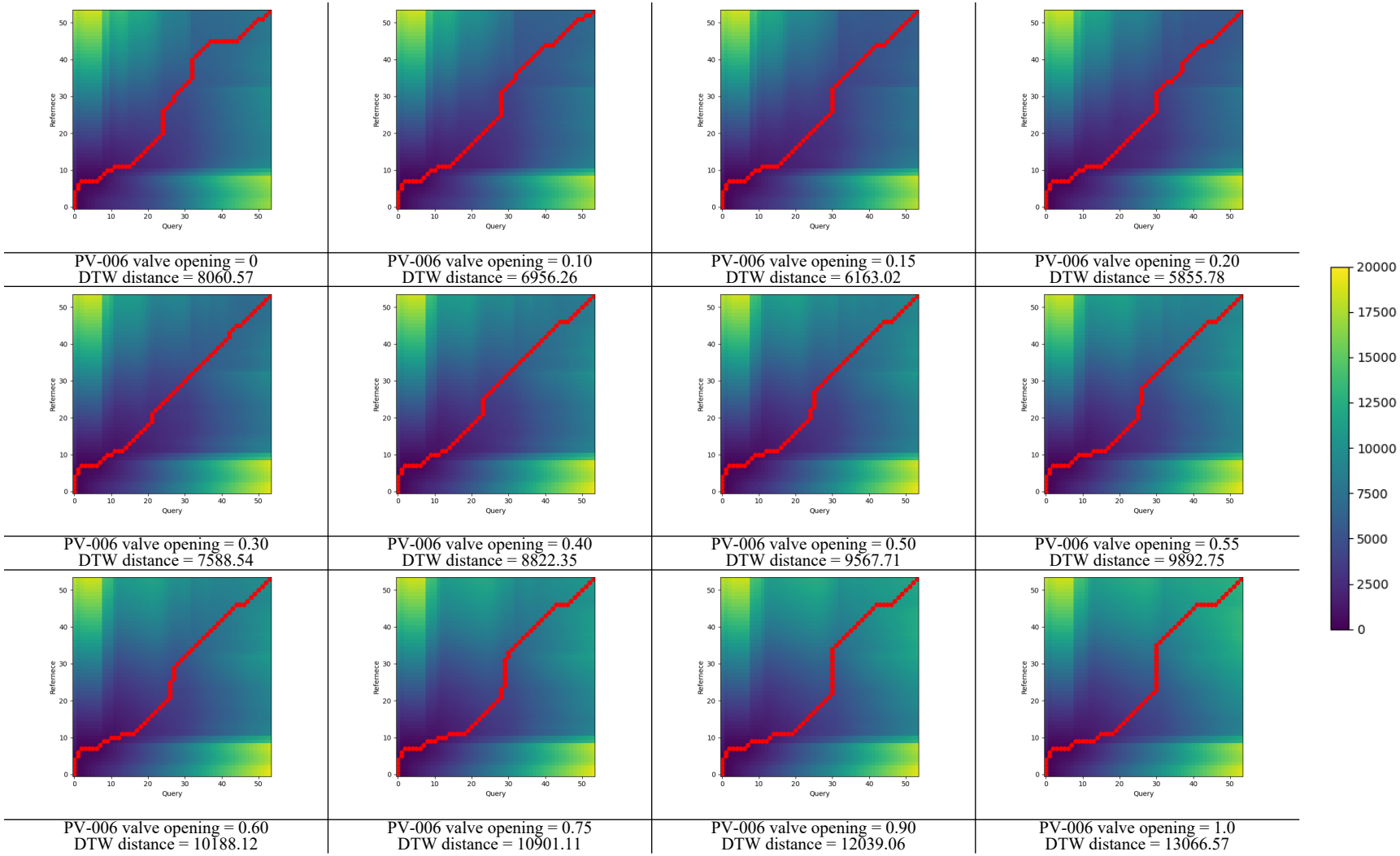

Figure 22. DTW map between multi-variate and experiment temperature data for TN-1-2, TS-1-1, TW-3-1, TC-201, TC-202, TC-006, TC-004 (i.e., reference data), and the Modelica simulation data (i.e., query data). The colors in each subplot represent the DTW distance between two datasets. The x- and y-axes represent the time indexes (1 time index = 300 seconds) for the query and reference data, respectively. The red line in each plot represents the optimal warping path.

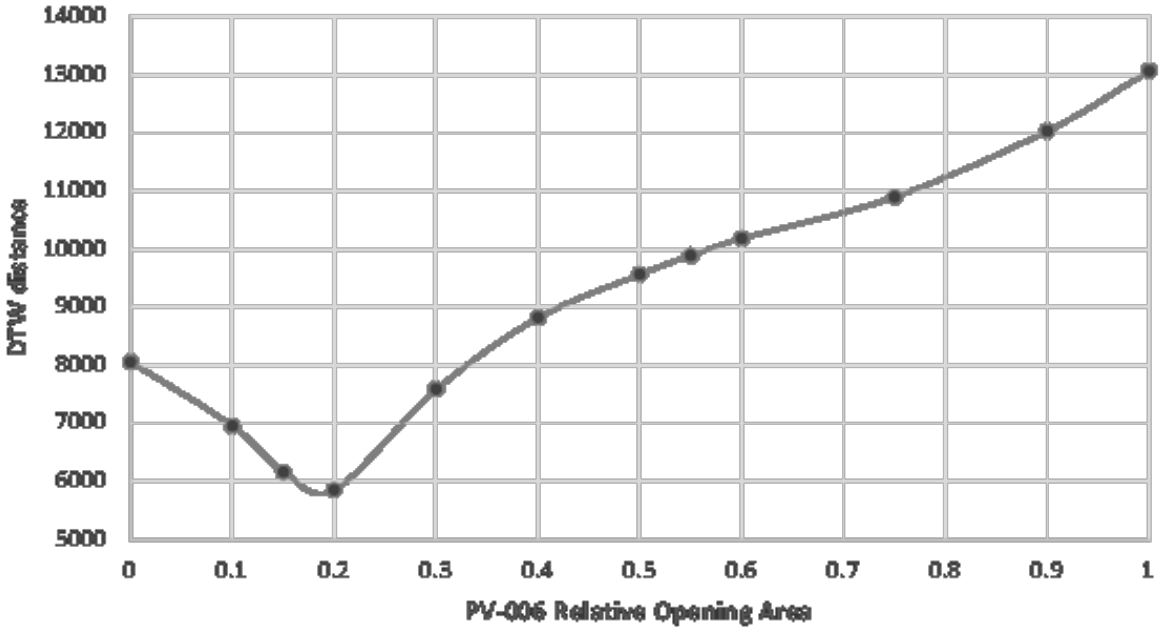

Figure 23. DTW distance profile over the PV-006 valve opening area.

6. Future Work

The first step of future work should aim at larger extent of experimental works, providing better characterization of the system. This is especially important with respect of the limits of the operation and thermocline tank performance and learning more about aspects of the system important for potential scale-up. Without supporting experimental data, any modelling work has only a limited value.

After that, multiple avenues of future work can be undertaken to enhance the modelling by updating it based on future changes made to the experimental facility. The first anticipated change to the facility is the installation of the PCU within MAGNET. The model will need to be verified after the installation is completed during fiscal year 2024.

Additional experiments designed to demonstrate consistent radial temperature and flow distributions within the thermocline tank can be used to characterize the value of improving the thermocline model so as to include the impacts of flow channeling. Significant value in adjusting the thermocline model is necessary to justify the addition of significant computational complexity. This activity can be revisited as future requirements are applied to DETAIL, including ones pertaining to digital twinning, remote operations, and uncertainty analyses.

If additional components that interface with existing systems are to be included in DETAIL, they must be added as they come online in the facility. As future INL projects are developed that require smaller-scaled proof-of-concept experiments that can be demonstrated at DETAIL, those options will be added to the HYBRID model.

The TEDS experiment provides opportunities to demonstrate thermal load mixing, thermocline storage performance, and simulated nuclear integrated energy systems operation. The Modelica model within the HYBRID repository has been shown in this work to accurately approximate the dynamic operation of TEDS. As operation shifts from MAGNET and TEDS to fully integrated DETAIL operation, further validation of the HYBRID model will be required. But with this additional validation, experimental demonstration of future nuclear integrated energy systems using non-nuclear operation can be analyzed.

7. CONCLUSION

INL's Integrated Energy Systems team continues to develop modelling tools for analyzing physical experimental systems. The experiments conducted within the DETAIL facility have been—and are intended to be—used to demonstrate practical dynamic applications for simulated nuclear heat generation. Through this work, the HYBRID modelling team provided verification (and eventually adjustment) of the models followed by validation against experimental data to provide the resulting models to other integrated energy systems teams (e.g., real-time optimization, control, and digital twins).

INL's HYBRID modelling team has successfully furthered the modelling of experimental systems at INL. The V&V activities have been successfully updated and demonstrated in relation to the TEDS experimental system. Parameters for an HX with limited information on internal configuration were tuned to match the vendor specifications. Metrics for comparing two time series of data (e.g., model and experimental) were updated and applied to compare experimental results with modelled data. The importance of first analyzing experimental data prior to using them further was highlighted in terms of two anomalies. The V&V tools were then practically demonstrated to validate a hypothesis regarding one of the anomalies in the experimental performance data by applying DTW to a single selected sensor reading, as well as to the combined results from multiple parameters within a relatively complex system.

ACKNOWLEDGEMENTS

This work was supported by the IES program at INL under DOE Operations contract no. DE-AC07-05ID14517.

REFERENCES

1. Frick, K. L., Bragg-Sitton, S. M., and Garrouste, M. (2021). "Validation and Verification for INL Modelica-based TEDS models Via Experimental Results." INL/EXT-21-64408, Idaho National Laboratory. https://doi.org/10.2172/1836100.
2. Frick, K. L. and Mikkelson, D. (2022). "HYBRID." [updated 2022 April 6; cited 2022 April 13]. Available at: https://www.github.com/idaholab/HYBRID.
3. Mikkelson, D. (2023). "HYBRID Modeling Validation and Verification Status Matrix." INL/RPT-23-03146, Idaho National Laboratory.
4. Frick, K. L., Bragg-Sitton, S. M., and Rabiti, C. (2020)."Development of the INL Thermal Energy Distribution System (TEDS) in the Modelica Eco-System for Validation and Verification." INL/EXT-20-59195, Idaho National Laboratory. https://doi.org/10.2172/1668777.
5. Stoots, C. M., et al. (2018). "Thermal Energy Delivery System Design Basis Report." INL/EXT-18-51351, Idaho National Laboratory. https://doi.org/10.2172/1756571.
6. Mikkelson, D., et al. (2022). "HYBRID Modeling of DETAIL Experimental Facility." INL/RPT-22-70396-Rev000, Idaho National Laboratory. https://doi.org/10.2172/1985489.
7. Guillen, D. P., and Wendt, D. (2020). "Integration of a Microturbine Power Conversion Unit in MAGNET." INL/EXT-20-57712, Idaho National Laboratory. https://doi.org/10.2172/1736010.

Appendix A

Appendix A

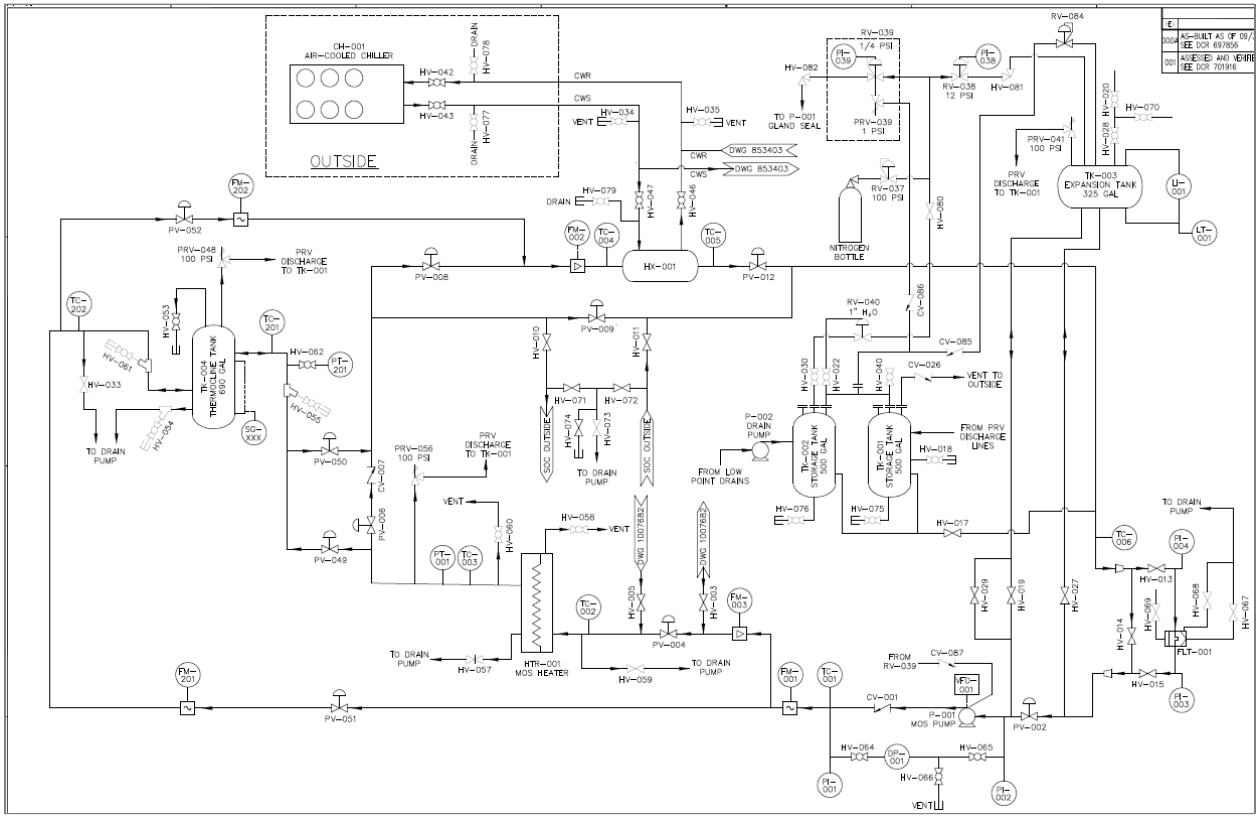

Figure A-1. P&ID of the TES system.

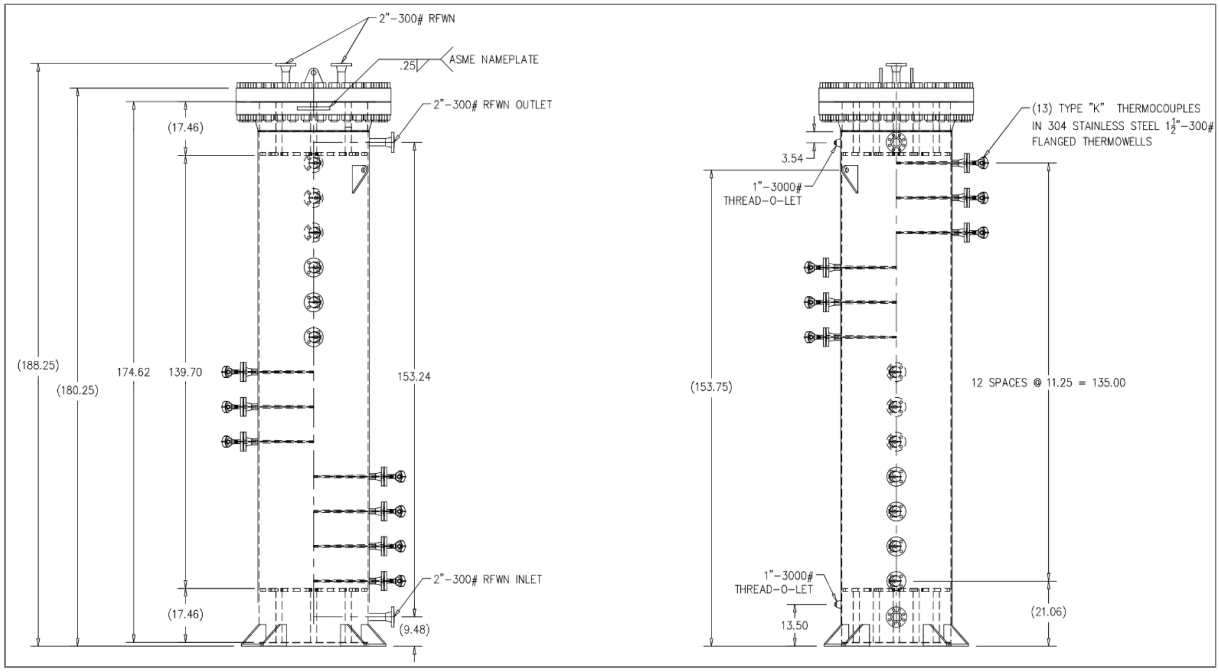

Figure A-2. Drawing of the thermocline tank, with the positions of the (multi-point) thermocouples.

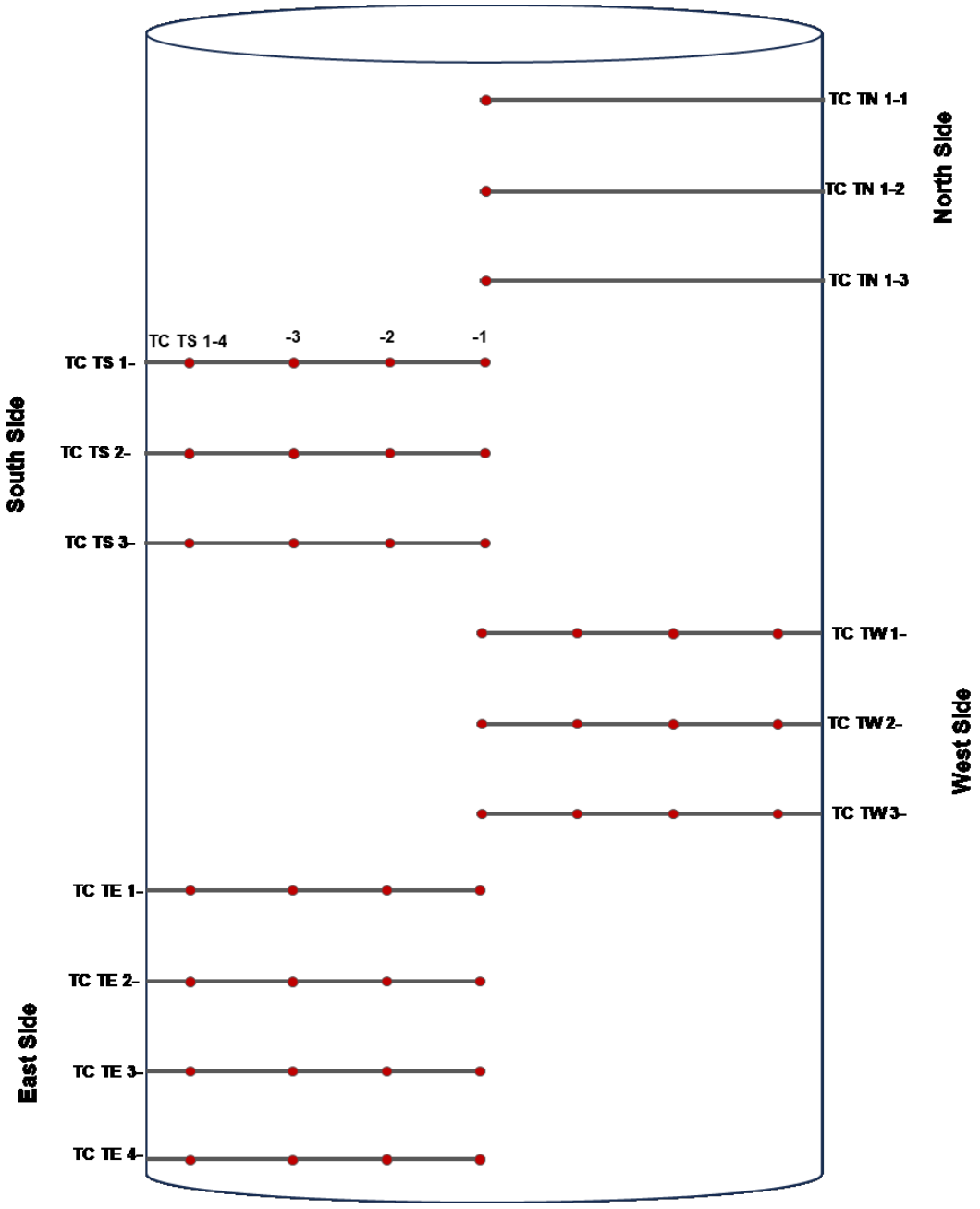

Figure A-3. Map of thermocouples within a thermocline tank.

Appendix B

Appendix B

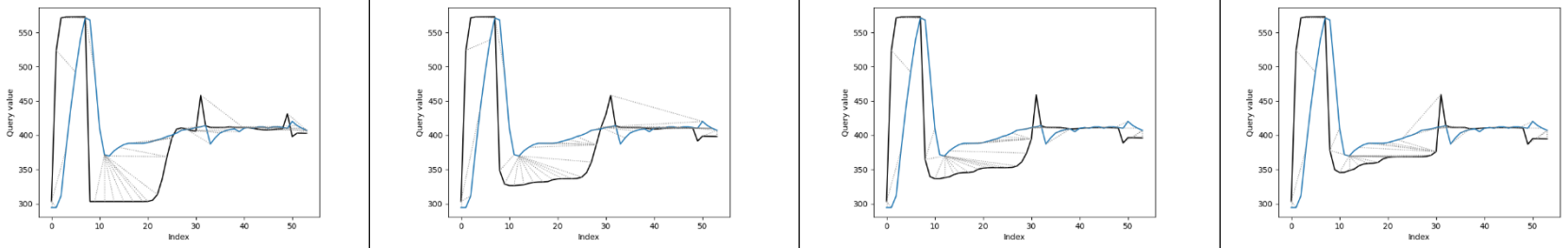

PV-006 valve opening = 0
dtw distance = 1968.15

PV-006 valve opening = 0.10
dtw distance = 1560.29

PV-006 valve opening = 0.15
dtw distance = 1271.30

PV-006 valve opening = 0.20
dtw distance = 1092.16

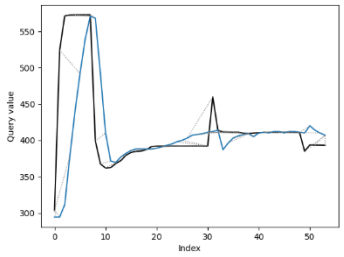

PV-006 valve opening = 0.30
dtw distance = 762.43

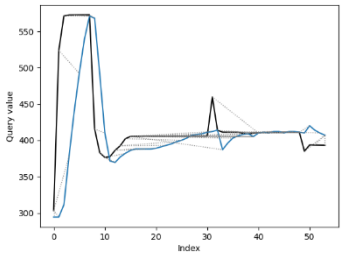

PV-006 valve opening = 0.40
dtw distance = 726.52

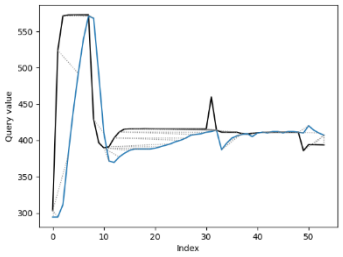

PV-006 valve opening = 0.50
dtw distance = 821.87

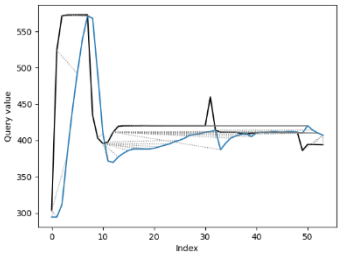

PV-006 valve opening = 0.55
dtw distance = 839.62

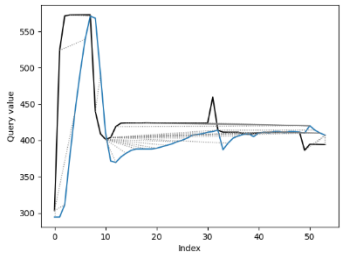

PV-006 valve opening = 0.60
dtw distance = 1011.46

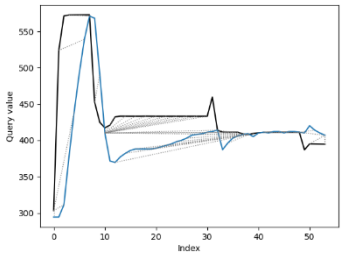

PV-006 valve opening = 0.75
dtw distance = 1425.38

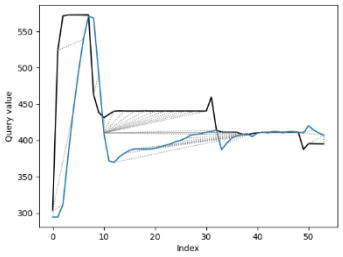

PV-006 valve opening = 0.90
dtw distance = 1590.00

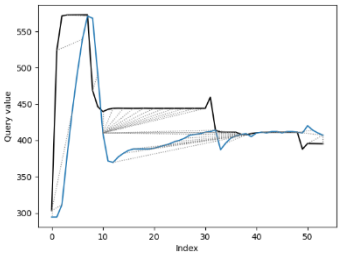

PV-006 valve opening = 1.0
dtw distance = 1679.31

Figure B-1. DTW distance between the simulation data (i.e., solid black line) and the experimental data (i.e., solid blue line) at the target location (i.e., TC-006). The x- and y-axes in each subplot represent the time index (1 index = 300 seconds) and temperature (K), respectively.

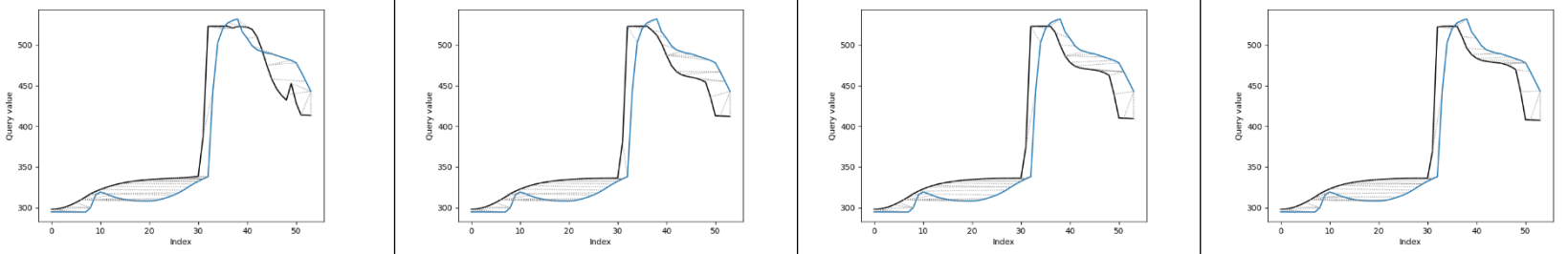

PV-006 valve opening = 0
dtw distance = 530.86

PV-006 valve opening = 0.10
dtw distance = 520.18

PV-006 valve opening = 0.15
dtw distance = 519.30

PV-006 valve opening = 0.20
dtw distance = 503.37

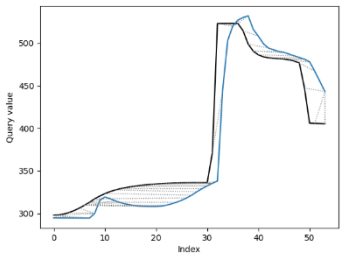

PV-006 valve opening = 0.30
dtw distance = 508.29

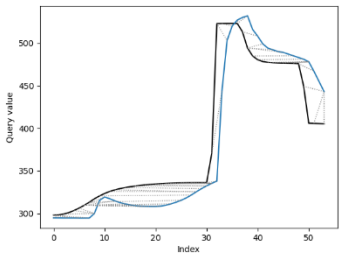

PV-006 valve opening = 0.40
dtw distance = 525.55

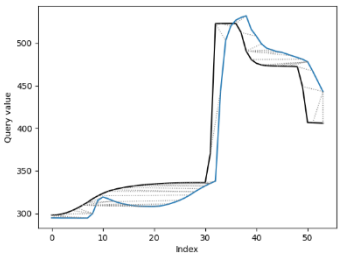

PV-006 valve opening = 0.50
dtw distance = 561.53

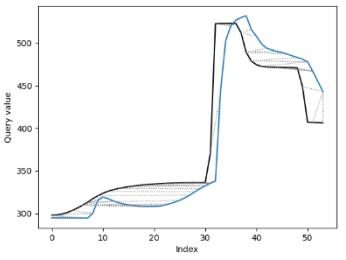

PV-006 valve opening = 0.55
dtw distance = 562.72

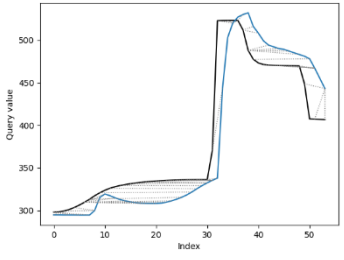

PV-006 valve opening = 0.60
dtw distance = 557.34

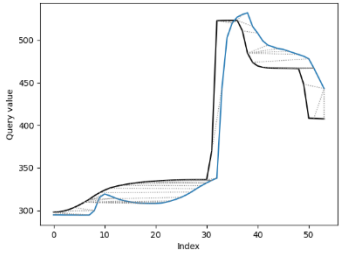

PV-006 valve opening = 0.75
dtw distance =542.70

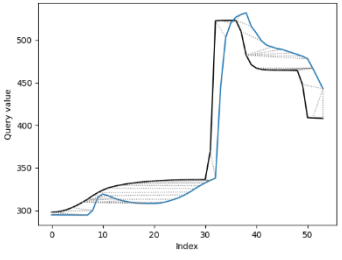

PV-006 valve opening = 0.90
dtw distance = 564.75

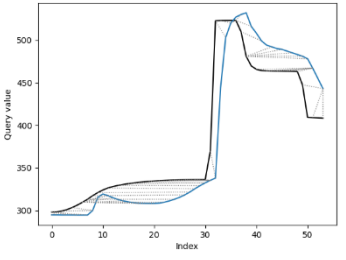

PV-006 valve opening = 1.0
dtw distance = 577.84

Figure B-2. DTW distance between the simulation data (i.e., solid black line) and the experimental data (i.e., solid blue line) at the target location (i.e., TC-004). The x- and y-axes in each subplot represent the time index (1 index = 300 seconds) and temperature (K), respectively.

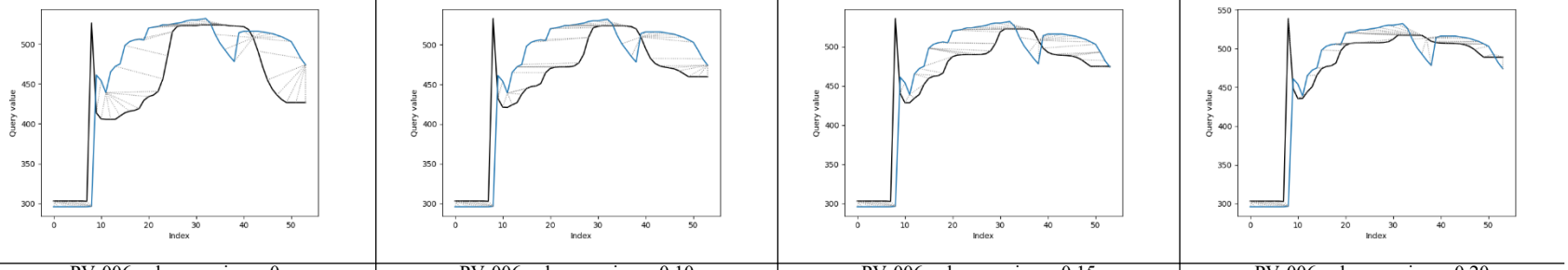

PV-006 valve opening = 0
dtw distance = 1352.67

PV-006 valve opening = 0.10
dtw distance = 769.84

PV-006 valve opening = 0.15
dtw distance = 713.83

PV-006 valve opening = 0.20
dtw distance = 667.03

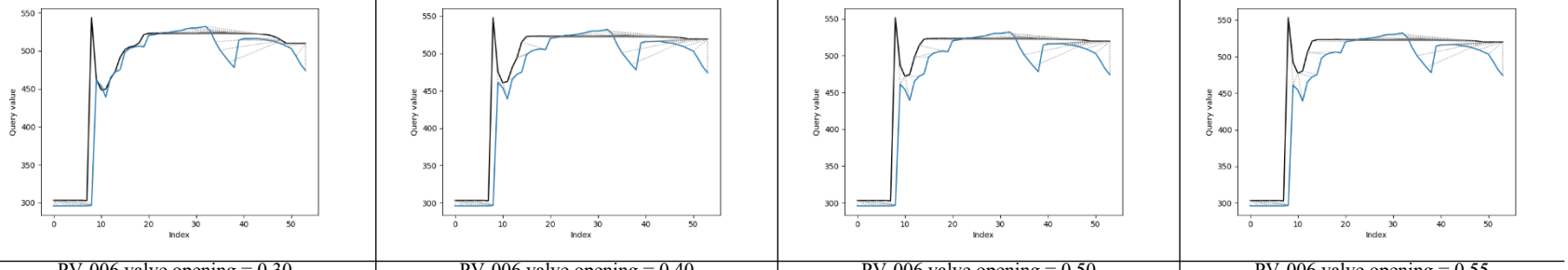

PV-006 valve opening = 0.30
dtw distance = 657.44

PV-006 valve opening = 0.40
dtw distance = 854.44

PV-006 valve opening = 0.50
dtw distance = 876.34

PV-006 valve opening = 0.55
dtw distance = 899.72

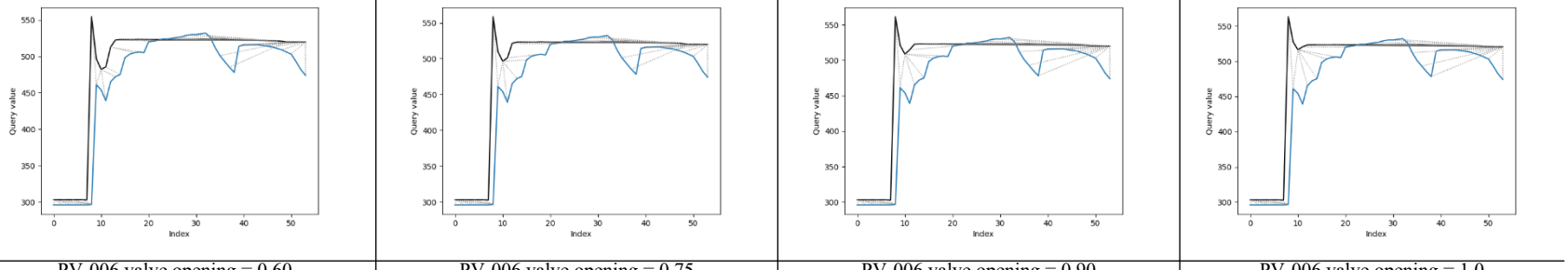

PV-006 valve opening = 0.60
dtw distance = 984.65

PV-006 valve opening = 0.75
dtw distance = 1040.71

PV-006 valve opening = 0.90
dtw distance = 1154.02

PV-006 valve opening = 1.0
dtw distance = 1236.55

Figure B-3. DTW distance between the simulation data (i.e., solid black line) and the experimental data (i.e., solid blue line) at the target location (i.e., TC-201). The x- and y-axes in each subplot represent the time index (1 index = 300 seconds) and temperature (K), respectively.

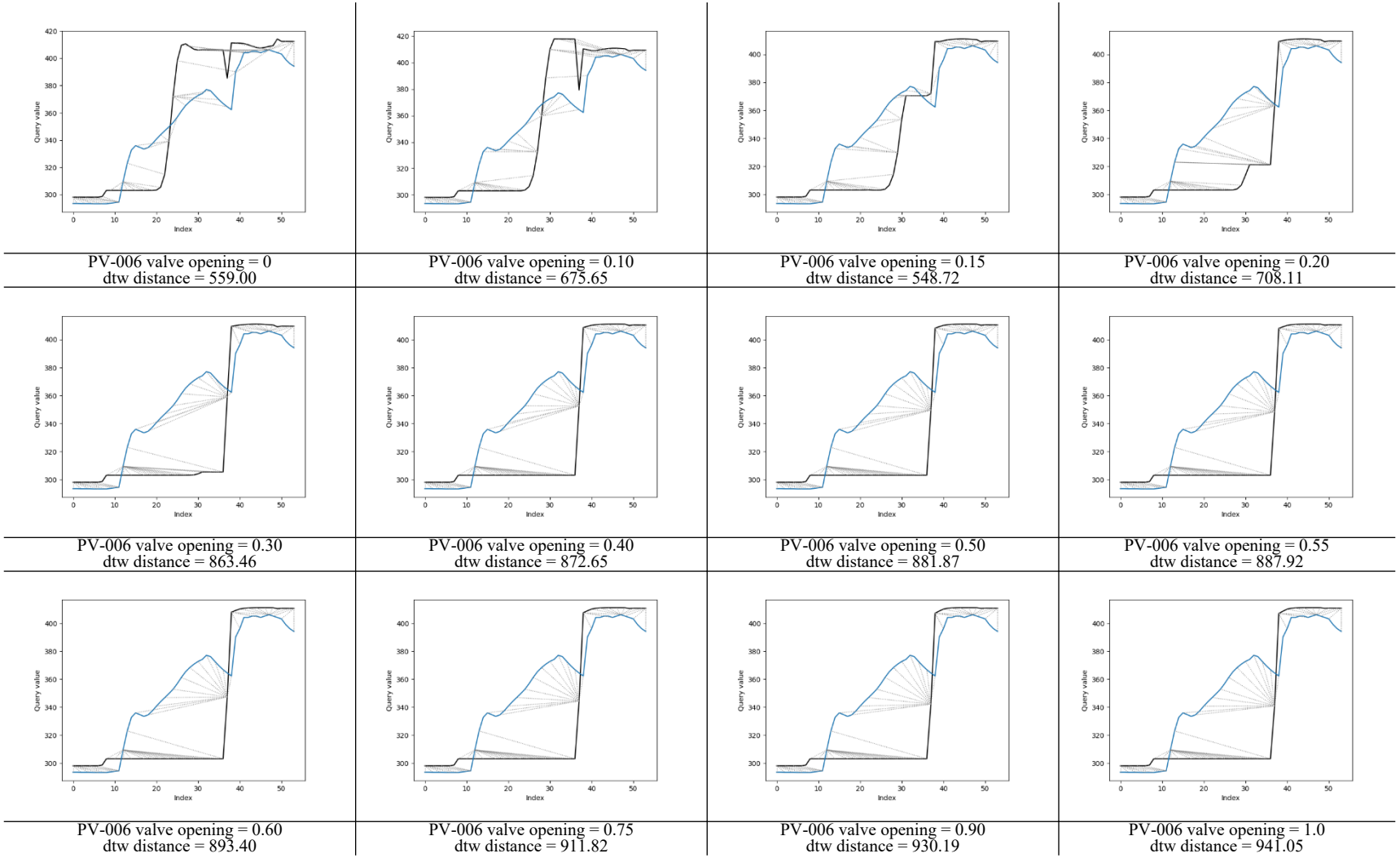

Figure B-4. DTW distance between the simulation data (i.e., solid black line) and the experimental data (i.e., solid blue line) at the target location (i.e., TC-202). The x- and y-axes in each subplot represent the time index (1 index = 300 seconds) and temperature (K), respectively.

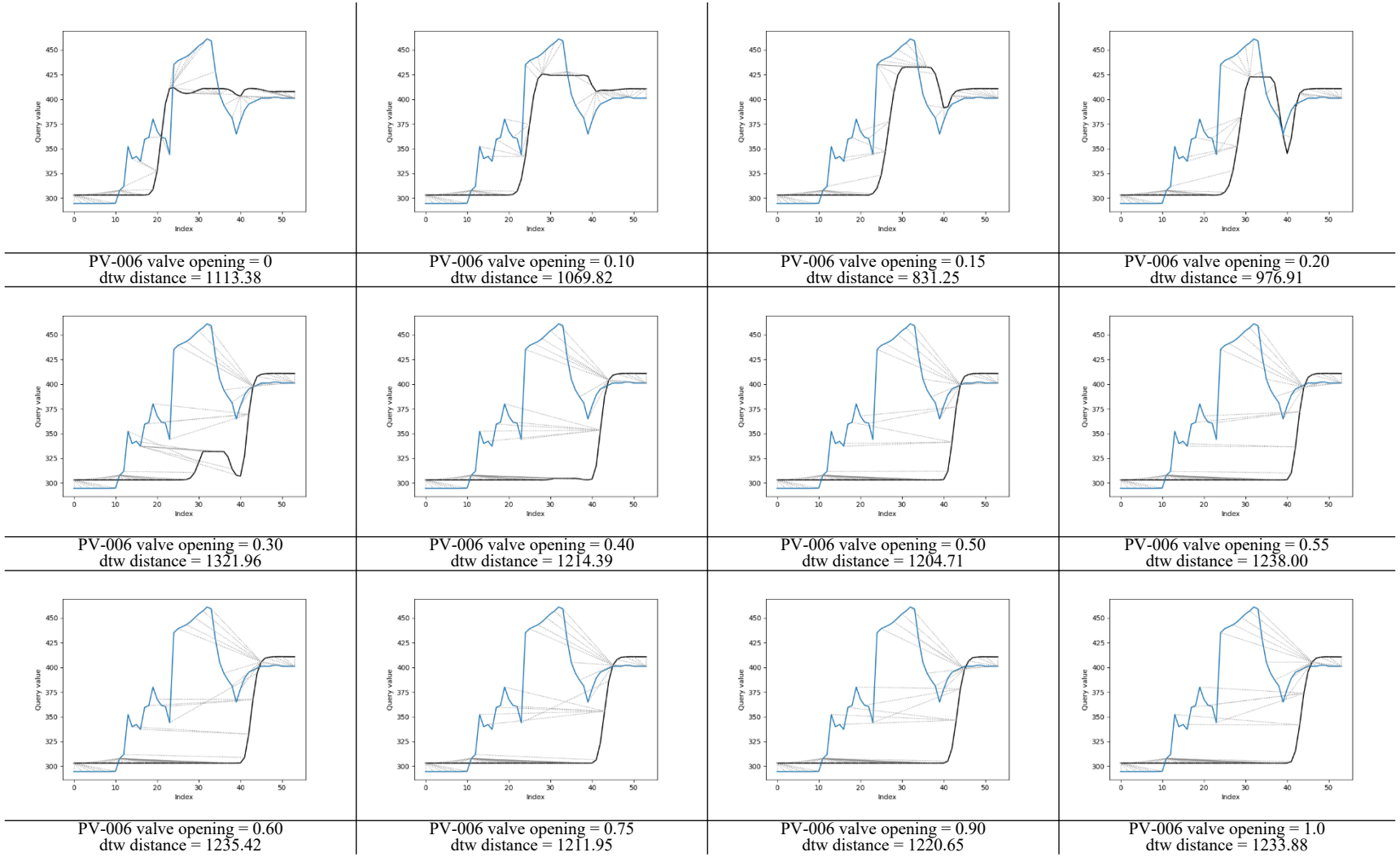

Figure B-5. DTW distance between the simulation data (i.e., solid black line) and the experimental data (i.e., solid blue line) for the thermocline temperature at the target location (i.e., TC TE-3-1). The x- and y-axes in each subplot represent the time index (1 index = 300 seconds) and temperature (K), respectively.

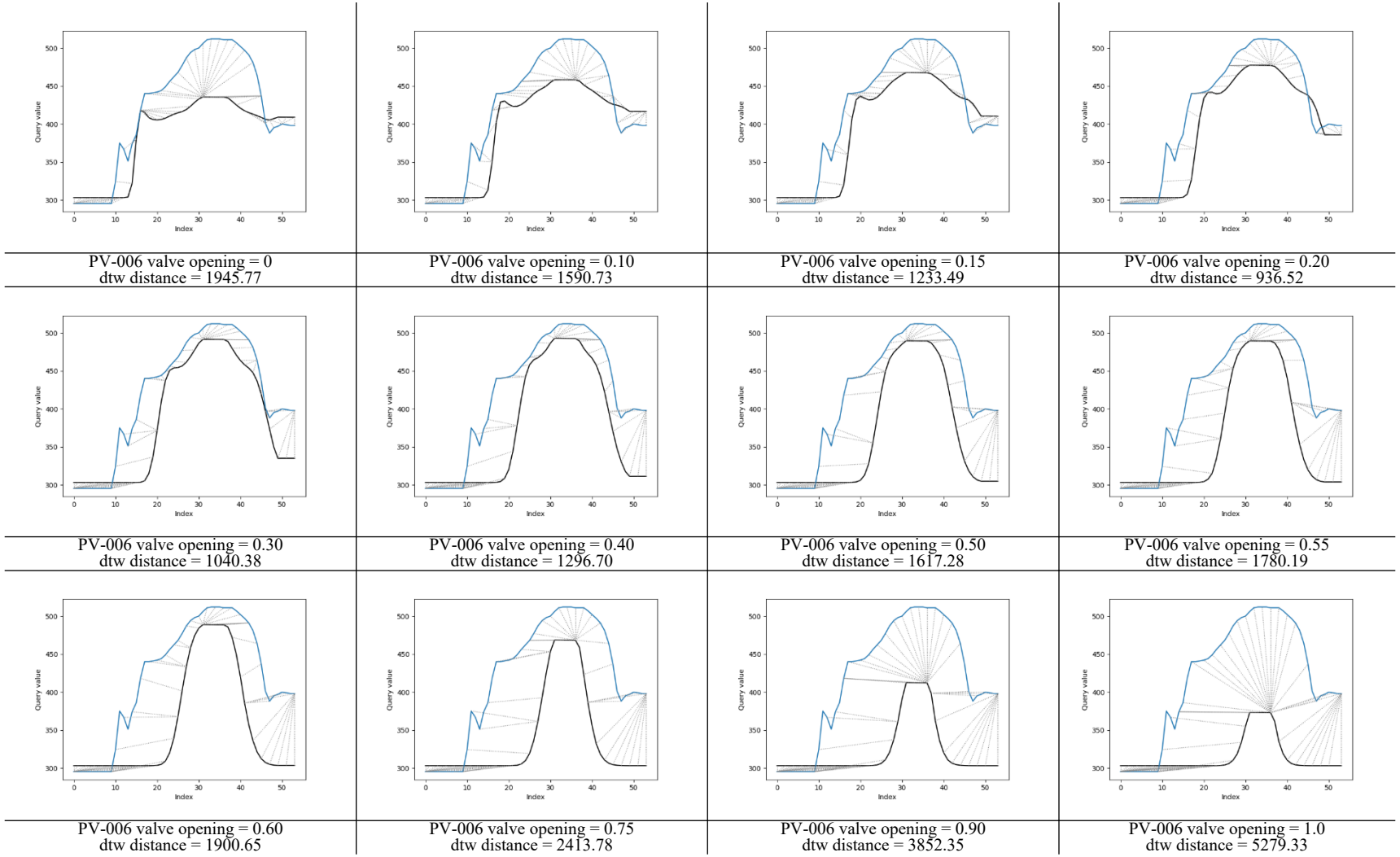

Figure B-6. DTW distance between the simulation data (i.e., solid black line) and the experimental data (i.e., solid blue line) for the thermocline temperature at the target location (i.e., TC TW-1-1). The x- and y-axes in each subplot represent the time index (1 index = 300 seconds) and temperature (K), respectively.